Published version available at: https://doi.org/10.1016/j.rse.2018.06.048

Assessing macrophyte seasonal dynamics using dense time series of medium resolution satellite data

Paolo VILLA[1,*], Monica PINARDI[1,2], Rossano BOLPAGNI[2], Jean-Marc GILLIER[3], Peggy ZINKE[4], Florin NEDELCUȚ[5], Mariano BRESCIANI[1]

[1] *Institute for Electromagnetic Sensing of the Environment, National Research Council, Milan, Italy*

[2] *Department of Chemistry, Life Sciences and Environmental Sustainability, University of Parma, Parma, Italy*

[3] *SNPN, Réserve naturelle du lac de Grand-Lieu, Bouaye, France*

[4] *Norwegian University of Science and Technology, Trondheim, Norway*

[5] *Dunărea de Jos University of Galati, Brăila, Romania*

* *corresponding author (villa.p@irea.cnr.it)*

Abstract

The improved spatial and temporal resolution of latest-generation Earth Observation missions, such as Landsat 8 and Sentinel-2, has increased the potential of remote sensing for mapping land surface phenology in inland water systems.

The ability of a time series of medium-resolution satellite data to generate quantitative information on macrophyte phenology was examined, focusing on three temperate shallow lakes with connected wetlands in Italy, France, and Romania.

Leaf area index (LAI) maps for floating and emergent macrophyte growth forms were derived from a semi-empirical regression model based on the best-performing spectral index, with an error level of 0.11 m^2 m^{-2}. Phenology metrics were computed from LAI time series using TIMESAT to analyze the seasonal dynamics of macrophyte spatial distribution patterns and species-dependent variability. Particular seasonal patterns seen in the autochthonous and allochthonous species across the three study areas related to local ecological and hydrological conditions.

How characteristics of the satellite dataset (cloud cover threshold, temporal resolution, and missing acquisitions) influenced the phenology metrics obtained was also assessed. Our results indicate that, with a full-resolution time series (5-day revisit time), cloud cover introduced a bias in the phenology metrics of less than 2 days. Even when the temporal resolution was reduced to 15 days (like the Landsat revisit time) the timing of the start and the peak of macrophyte growth could still be mapped with an error of no more than 2-3 days.

Keywords: vegetation phenology; LAI; shallow lakes; spectral indices; Sentinel-2; Landsat 8.

Received 3 October 2017, Accepted 27 June 2018, Available online 11 July 2018 (**embargo expires 11 July 2020**)

Published version available at: https://doi.org/10.1016/j.rse.2018.06.048

1. Introduction

Although much has been learned about the long-term effect of climate change on the phenology of terrestrial ecosystems (Richardson et al., 2013; Yang et al., 2015), there is still little information available on aquatic ecosystems, and even less regarding aquatic plants. It is essential to improve our understanding of seasonal changes in macrophyte growth in order to shed light on the ecological drivers of aquatic system degradation, and promote effective conservation programs. Some studies have examined emergent macrophytes (Alahuhta et al., 2011), floating plants (Peeters et al., 2013), and their interaction with submerged macrophytes (Netten et al., 2011; Li et al., 2017). These studies were based largely on existing thematic cartography and *in situ* observations of vegetation density and biomass, so their conclusions are not generalizable across spatial and temporal scales. As recently stressed by Luo et al. (2016), large lakes and wetland ecosystems are difficult to survey, and that is why few data have been collected on the temporal dynamics of aquatic vegetation. Consistent, spatialized details of key phenological features, such as the timing of the start and end of the growing season, are needed to elucidate the main drivers behind the seasonal dynamics of aquatic vegetation (Wang et al., 2012; Sletvold and Ågren, 2015). A detailed knowledge of the seasonal dynamics of macrophyte communities is crucial to our understanding of the role in time and space of different functional groups, the competition with other primary producers (Bolpagni et al., 2014; Villa et al., 2015; Zhang et al., 2015), and the potential impact of invasive species (Wolkovich and Cleland, 2011). Furthermore, managers of natural resources and policy-makers demand increasingly extensive temporal and spatial information on phenological dynamics in order to address important issues relating to global environmental change (White and Nemani, 2003; Cleland et al., 2007). In this setting, remote sensing has virtually ideal features in terms of spatial and temporal resolution, synoptic view and coverage, sensitivity to the structural and physiological features of vegetation, sampling rate, and repeatability (Malthus, 2017). Long-term, consistent satellite data can be used to monitor and quantify intra- and inter-annual trends in vegetation cycles (e.g. Villa et al., 2012; Fensholt et al., 2015). A large corpus of scientific literature on remote sensing applied to land surface phenology has been accumulated in the last decade, focusing particularly on terrestrial biomes (e.g. Reed et al., 1994; Zhang et al., 2003; Fisher and Mustard, 2007). Most of the studies used satellite data with a medium to low resolution, i.e. a pixel size larger than 1 km (e.g. Jenkins et al., 2002; Reed, 2006; Fisher et al., 2007). The particular characteristics of macrophytes (e.g. background conditions, canopy structures) and their ecosystems (mostly bodies of shallow water, with small surface areas and a great variety of plant species and forms) make them difficult to study using data with a coarse spatial resolution, and the techniques developed for terrestrial plants would need to be adapted and/or reparametrized. Some phenological analyses were conducted on macrophytes using the 30 m spatial resolution of the Landsat sensors (e.g. Hestir et al., 2015; Luo et al., 2016), but the 16-day revisit time could not ensure a sufficiently-detailed

Received 3 October 2017, Accepted 27 June 2018, Available online 11 July 2018 (**embargo expires 11 July 2020**)

Published version available at: https://doi.org/10.1016/j.rse.2018.06.048

monitoring of the variability in macrophyte growth over time.

In July 2017, the Sentinel-2 satellite constellation managed by the ESA through the Copernicus initiative started to provide high-quality data with a 10-20 m resolution and a 5-day revisit time (Drusch et al., 2012). These characteristics make the Sentinel-2 data a powerful tool for monitoring macrophytes and their seasonal dynamics with a hitherto unknown level of detail.

This paper analyzes the capabilities of such a dense time series (with a 5- to 10-day revisit time) of medium-resolution (10-30 m) satellite data to provide information and metrics of macrophyte phenology. Data were collected and analyzed over three shallow European lakes with connected wetlands that host macrophyte communities of floating and emergent species common to temperate freshwater ecosystems. In particular, our objectives were: i) to calibrate a semi-empirical model for deriving leaf area index (LAI) time series for floating and emergent macrophytes from satellite spectral reflectance data; ii) to map the macrophyte phenology metrics across our study areas, comparing their spatial distribution and species-dependent variability; iii) to examine how characteristics of the satellite dataset – i.e. maximum cloud cover, temporal resolution, and missing acquisitions – influenced the phenology metrics obtained.

Table 1. Key characteristics of the main target, floating and emergent macrophyte species in the study areas.

Study area	***Species* (common name)**	**Functional group**[1]	**Abundance**	**Origin of species**
Mantua lakes system	*Nelumbo nucifera* (sacred lotus)	emergent rhizophyte	dominant (Superior Lake)	allochthonous
	Trapa natans (water chestnut)	free-floating pleustophyte	dominant (Middle and Inferior lakes)	autochthonous
	Nuphar lutea (yellow water lily)	floating-leaved rhizophyte	spread patches (all lakes)	autochthonous
	Nymphaea alba (white water lily)	floating-leaved rhizophyte	small patches (Middle Lake)	autochthonous
	Nymphoides peltata (yellow floating heart)	floating-leaved rhizophyte	small patches (Vallazza wetland)	autochthonous
	Ludwigia hexapetala (water primrose)	floating rhizophyte	spreading (Superior and Middle lakes)	allochthonous
Lac de Grand Lieu	*Nuphar lutea* (yellow water lily)	floating-leaved rhizophyte	co-dominant	autochthonous
	Nymphaea alba (white water lily)	floating-leaved rhizophyte	co-dominant	autochthonous
	Nymphoides peltata (yellow floating heart)	floating-leaved rhizophyte	small patches	autochthonous
	Trapa natans (water chestnut)	free-floating pleustophyte	small patches	autochthonous
	Ludwigia hexapetala (water primrose)	floating rhizophyte	spreading (riparian areas)	allochthonous
	Ludwigia peploides (creeping water primrose)	floating rhizophyte	spreading (riparian areas)	allochthonous
Fundu Mare island	*Nymphaea alba* (white water lily)	floating-leaved rhizophyte	co-dominant	autochthonous
	Trapa natans (water chestnut)	free-floating pleustophyte	co-dominant	autochthonous
	Nymphoides peltata (yellow floating heart)	floating-leaved rhizophyte	small patches	autochthonous

[1] according to Villa et al. (2015).

Received 3 October 2017, Accepted 27 June 2018, Available online 11 July 2018 (**embargo expires 11 July 2020**)

Published version available at: https://doi.org/10.1016/j.rse.2018.06.048

1. Study areas

Three shallow freshwater bodies were considered, with their connected wetlands, which host macrophyte communities mainly comprising floating and emergent species (Table 1). The three areas share a temperate climate and are located in different parts of Europe. The Mantua lakes system (Italy) was the principal study area, where *in situ* data were extensively collected for the purpose of implementing our analysis. The Lac de Grand-Lieu (France), and Fundu Mare Island (Romania) are test sites for which less reference information was available.

1.1.Mantua lakes system

The Mantua lakes system lies in the Po river floodplain in northern Italy (45°10' N, 10°47' E; Figure 1c), with a continental climate (Peel et al., 2007). The Superior, Middle and Inferior lakes are semi-artificial, created by dams installed on the Mincio River in the 12th century. The three fluvial lakes are small in surface area (~ 6 km^2), shallow (with an average depth of 3.5 m), and hypertrophic (with chlorophyll-a concentrations up to 100 µg L^{-1}). The water level in the Superior Lake remains constant (at 17.5 m a.s.l.) because water outflow is regulated by the Vasarone and Vasarina sluice gates (Pinardi et al., 2015). In the Middle and Inferior lakes, water levels are allowed to vary within a very narrow range (14.0-14.5 m a.s.l.) for safety reasons (to avoid flooding in the historical city center). The lakes are protected and form part of a Regional Natural Park. They are surrounded by two wetlands, called Valli del Mincio (VM) and Vallazza (VW), which are nature reserves. The Mantua lakes system is characterized by phytoplankton coexisting with macrophyte communities (Pinardi et al., 2011; Bolpagni et al., 2014; Villa et al., 2015). During the period from April to October, dense stands of an allochthonous emergent rhizophyte, *Nelumbo nucifera*, colonize the Superior Lake, together with some small patches of autochthonous floating species, *Nuphar lutea* and *Trapa natans*. The Middle Lake hosts dominant monospecific stands of *T. natans*, with small patches of nymphaeids (*N. lutea* and *Nymphaea alba*). The Inferior Lake mainly hosts small, isolated *T. natans* beds. In recent years, *Ludwigia hexapetala*, a very invasive, mat-forming allochthonous species, has spread in the littoral zones of the Superior and Middle lakes.

1.2. Lac de Grand-Lieu

The Lac de Grand-Lieu is a large, eutrophic, shallow freshwater lake in north-western France (Loire-Atlantique department, 47°05' N, 1°41' W; Figure 1a), 25 km from the Atlantic coast. It extends over 63 km² in winter, when the wet meadows, reed beds, and tree groves (*Salix* spp., *Alnus* spp.) are flooded. Water level fluctuations follow seasonal precipitation, but have been artificially managed since the early 1960s by means of a sluice gate downstream from the lake. In spring, the water level drops by one meter on average with respect to the annual maximum. In summer, the sluice gates are shut and the water level drops slowly due to evaporation until it rains in autumn. Depending on the year, the lake's level may drop

Received 3 October 2017, Accepted 27 June 2018, Available online 11 July 2018 (**embargo expires 11 July 2020**)

Published version available at: https://doi.org/10.1016/j.rse.2018.06.048

by 15 to 35 cm between July and October. The permanently flooded central area (21 km^2) is about one meter deep, and partially covered with floating-leaved macrophytes (~ 7 km²), especially *N. alba* and *N. lutea*. Small beds of *T. natans* and *Nymphoides peltata* extend over areas of 0.1 to 0.3 km^2, respectively (Gillier and Reeber, 2016). As in other wetlands nearby (Haury et al., 2011), the invasive, allochthonous *L. hexapetala* and *Ludwigia peploides* have spread widely in the channels and on the mudflats around the edge of the central area, expanding in a more "terrestrial" form on the wet meadows and sparse reed beds.

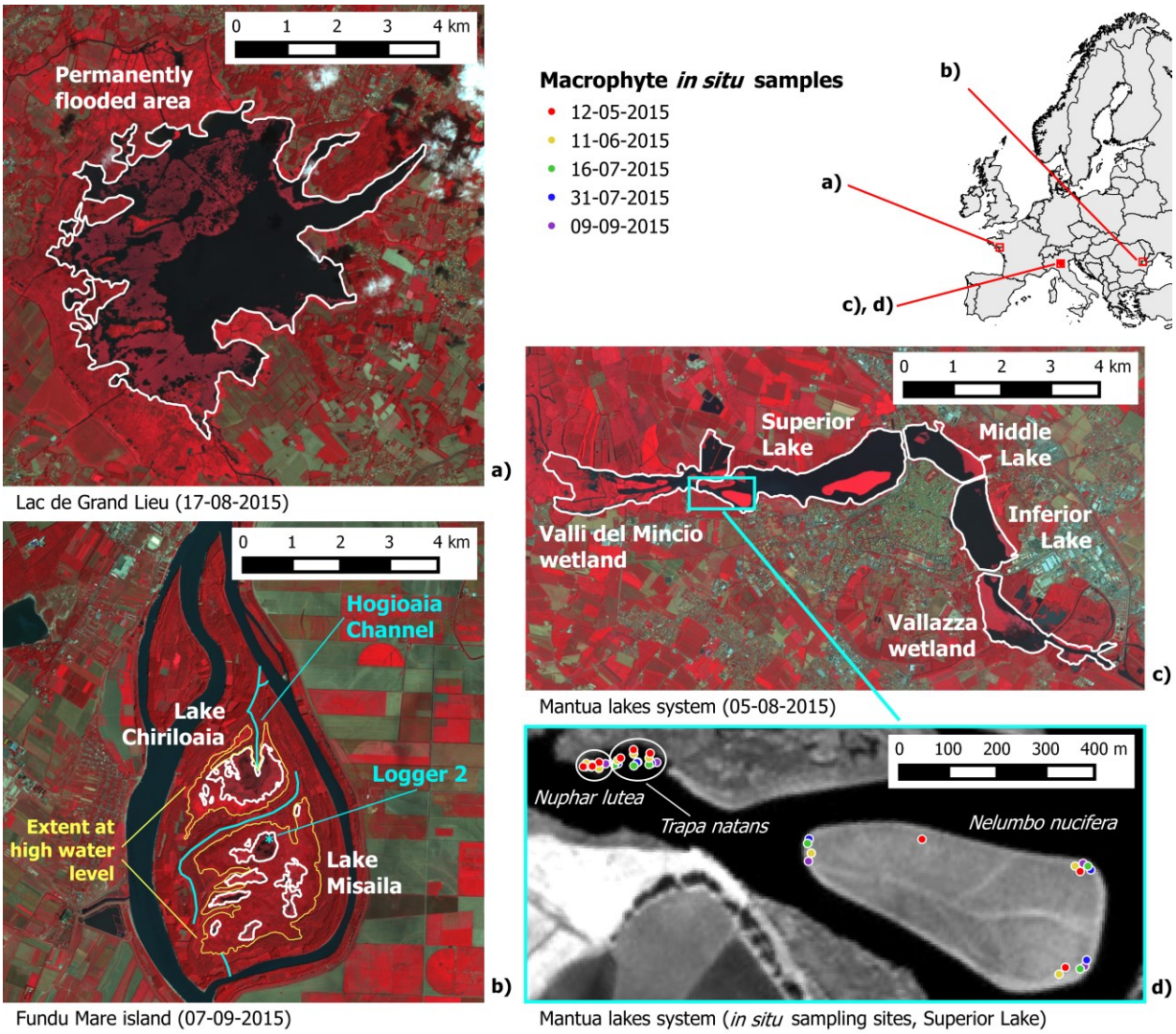

Figure 1. Study areas shown as SPOT5 images in color infrared RGB combination at peak of macrophyte growth: a) Lac de Grand-Lieu (France); b) Fundu Mare Island (Romania); c) Mantua lakes system (Italy); d) detail of area of Mantua lakes system with sites (see Table 1 for coordinates) where macrophyte samples were collected in 2015 (NIR band shown in greyscale).

1.1. Fundu Mare Island

Fundu Mare Island, in eastern Romania (45°11' N, 27°57' E; Figure 1b), is part of the lower Danube

Received 3 October 2017, Accepted 27 June 2018, Available online 11 July 2018 (**embargo expires 11 July 2020**)

Published version available at: https://doi.org/10.1016/j.rse.2018.06.048

River system, and one of few remaining floodplain islands still in a nearly natural state. It is part of the Small Wetland of Braila (SWB) natural park, which is an internationally important bird sanctuary. Fundu Mare Island is the northernmost of seven islands in the SWB. It covers an area of 19.5 km^2, about half of which is regarded as an aquatic habitat, consisting of two main shallow bodies of water: Lake Chiriloaia (3 km^2) and Lake Misaila (6.3 km^2) (SWB 2015). The lakes reach their maximum expansion in spring, when the River Danube reaches its peak volume. The water level then drops over subsequent months, depending on the level of the Danube, weather conditions, and how weirs on the outlet channels are managed (Zinke et al., 2016).

The climate at Fundu Mare is warm, humid and continental (Peel et al., 2007). The dominating types of vegetation include floodplain forests comprising the riparian species *Salix* spp., *Populus* spp., helophytes (*Phragmites australis*, *Schoenoplectus lacustris*) and aquatic macrophytes, with *N. alba* and *T. natans* as the dominant species, and some *N. peltata*. In the last few years, willow (*Salix* spp.) has massively encroached on some formerly open areas, with negative consequences for fish and birds (Zinke et al., 2016).

2. Dataset

2.1. Field data for the Mantua lakes system

In situ sampling campaigns were conducted by boat during the 2015 vegetation period (on 12 May, 11 June, 16 and 31 July, and 9 September) in the Mantua lakes system, collecting samples of *N. lutea* (NL), *T. natans* (TN), and *N. nucifera* (NN) for a total of 45 plots (three species sampled at three sites, with replicates, on five different dates). At each sampling site, the plot represents an area of around 10 x 10 m (consistent with the satellite data resolution) evenly covered with a given species.

For each macrophyte plot, *in situ* georeferenced (Trimble GeoXM) photographs were taken (with a Sony DSC-HX60 RGB camera; three photos for each plot) from the nadir, about 1 m above the canopy, framing a 1 x 1 m floating square plot. The macrophyte LAI (m^2 m^{-2}) was derived for each image by manually marking the areal size of each leaf falling within the framed plot (taking overlapping leaves into account). As reported by Villa et al. (2017), this method has proved more accurate for floating and floating-leaved species than for species with emerging leaves (*N. nucifera*). As the present work focused on plant growth over time, a slight underestimation of the LAI in absolute terms for a single species was not considered a limitation for the purposes of analyzing the seasonal dynamics at ecosystem level, which relies on charting the relative LAI curve across the growing season.

Spectral response data for different surfaces, including terrestrial and aquatic targets, were acquired *in situ* to examine the radiometric accuracy and consistency of the processed satellite data (for details, see the Supplementary Material).

Received 3 October 2017, Accepted 27 June 2018, Available online 11 July 2018 (**embargo expires 11 July 2020**)

Published version available at: https://doi.org/10.1016/j.rse.2018.06.048

2.2. Satellite data

Medium-resolution (10-30 m on the ground per pixel), broadband multi-spectral (visible in the shortwave infrared range) satellite data were collected over the three areas, following seasonal changes in the macrophytes for the year 2015. The bulk of this dataset consisted of images acquired during the SPOT5 (Take5) experiment, when data were collected over 150 sites every 5 days, under a fixed geometry, from April to September 2015. The aim of the SPOT5 (Take5) was to simulate the acquisition of time series that the ESA's full Sentinel-2 constellation would start to provide once both its satellites were operational (in July 2017). Landsat 7 and Landsat 8 images acquired before April 2015, and Sentinel-2A images acquired after September 2015 were also examined to complete the time series so that it covered the whole of 2015. The whole dataset (Figure 2) consisted of 33 images obtained over the Mantua lakes system (plus 12 used to check time series consistency), 27 over the Lac de Grand-Lieu, and 29 over Fundu Mare Island.

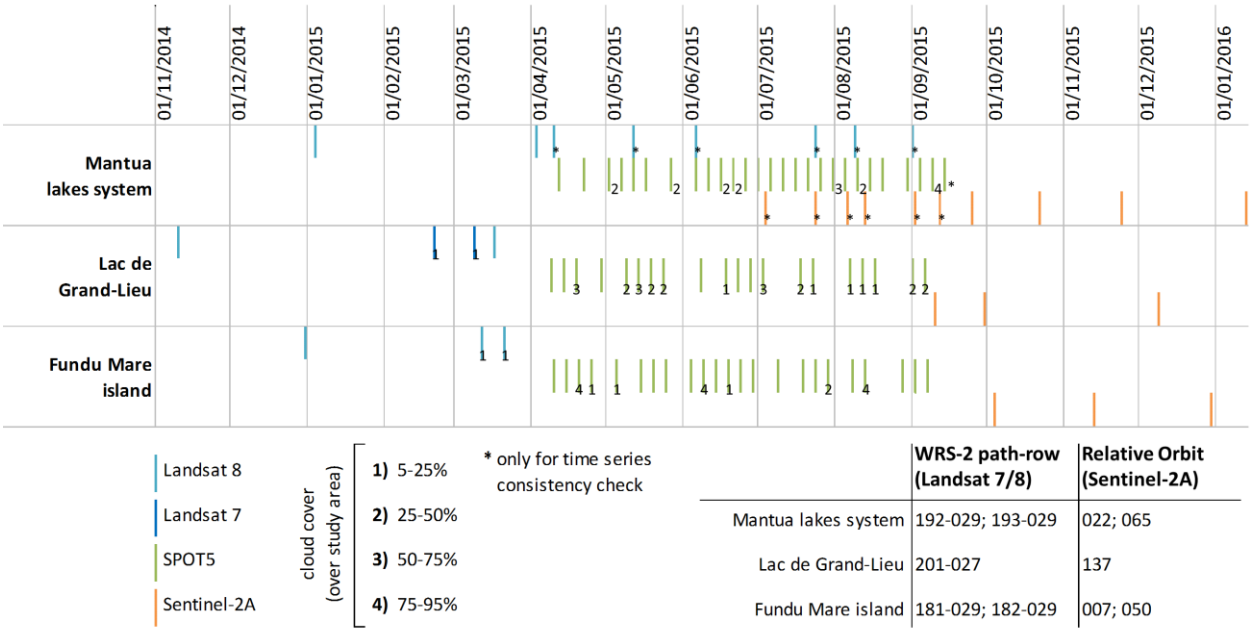

Figure 2. Characteristics of the satellite dataset.

2.3.Ancillary data

At the Lac de Grand-Lieu, floating-leaved plants are monitored every three years by acquiring high-resolution aerial RGB photos of the permanently flooded area and its surroundings (Figure 1a). In 2015, this survey was conducted on 8 August, in good weather conditions. To ensure consistency with the findings of previous surveys, the ortho-rectified images obtained in 2015 were resampled at a 0.5 m ground resolution and cropped to fit the area covered by floating and emergent macrophyte beds. In the resulting map, the main class included *N. lutea* and *N. alba*, while the other classes were *T. natans*, *N.*

Received 3 October 2017, Accepted 27 June 2018, Available online 11 July 2018 (**embargo expires 11 July 2020**)

Published version available at: https://doi.org/10.1016/j.rse.2018.06.048

peltata, and *S. lacustris*. The areas covered by these four vegetation classes were digitized with a geographic information system (Quantum GIS).

Fundu Mare Island was inspected on 8 May, 8 June and 21 December 2015, and a thorough field survey was conducted between 9 and 16 July 2015 to shed light on the island's hydrological processes. Between 9 June and 21 December 2015, the water level was recorded at three sites in the lakes using pressure sensors (Global Water). The water level upstream from the weir on the main outlet channel (Hogioaia channel, Figure 1b) was measured on four different dates and its fluctuations between these dates was estimated from the water balance (Zinke et al. 2016). Figure 3 shows the water levels in 2015, with reference to the Black Sea Sulina geodetic datum (i.e. a.s.l.), and the typical depths of the water under different macrophyte communities characterizing the site.

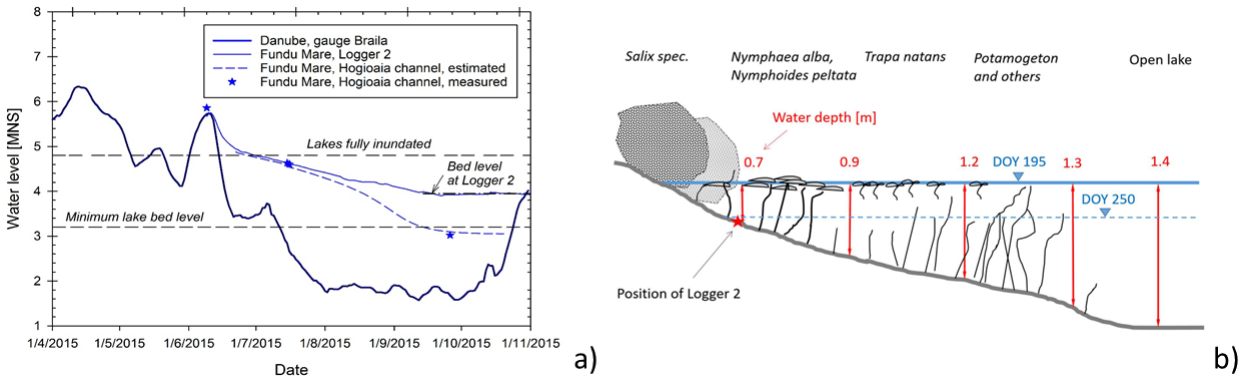

Figure 3. Relationships between macrophytes and hydrology on Fundu Mare Island: a) water levels of the Danube (gauge in the city of Braila: 45°16'N, 27°57'E), Lake Misaila (Logger 2, Figure 1b), and upstream from the weir (Hogioaia channel, Figure 1b). Note that the seasonal maximum water level in the winter of 2015 was higher than the average level for the Island's lakes when fully flooded (~4.8 m a.s.l.). In the summer of 2015, the water level for lake Misaila dropped below that of the bed at the site of the logger (3.9 m a.s.l.); b) typical depths of water measured under different macrophyte communities during the field survey at 4.6 m a.s.l. on 14 July 2015 (DOY 195), also showing the position of Logger 2 in Lake Misaila, and the water level on 7 September 2015 (DOY 250).

During the field activities, the status of the vegetation was documented by means of georeferenced photos taken with a RGB digital camera (Olympus, with GPS tagging), and field notes on the types of community and species. On 13 and 14 July 2015, the water levels measured at selected locations for Lakes Chiriloaia and Misaila (Figure 1b) ranged between 0.7 and 1.5 m (Figure 3b). Overall plant cover was documented in September 2015 during a survey conducted with an unmanned aerial vehicle (UAV; Parrot SenseFly eBee), mounted with a high-resolution digital camera (Canon IXUS 127 HS; 16.1 Mpixels). Approximately 8,000 photos were taken from a height of around 200 m, covering an area of 20 km^2, with a nominal pixel size varying between 2 and 5 cm on the ground. These photos were then used to generate an RGB orthomosaic of the whole area.

3. Methods

Received 3 October 2017, Accepted 27 June 2018, Available online 11 July 2018 (**embargo expires 11 July 2020**)

Published version available at: https://doi.org/10.1016/j.rse.2018.06.048

3.1.Satellite data pre-processing

SPOT5 data were retrieved from the ESA-CNES web portal (https://spot-take5.org) for the three sites of interest, namely: 'Italia: Mantua' (Mantua lakes system), 'France: Pornic' (Lac de Grand-Lieu), and 'Romania: Braila' (Fundu Mare Island). The SPOT5 data were retrieved as Level 2A products (10-20 m resolution for multispectral bands), ortho-rectified for surface reflectance, and corrected for atmospheric effects (including adjacency) using the Multi-sensor Atmospheric Correction and Cloud Screening processor (MACCS; Hagolle et al., 2015).

Landsat images (30 m resolution for multispectral bands) were pan-sharpened at 15 m resolution using the Gram-Schmidt method (Laben and Brower, 2000). For the Landsat 7 data, SLC-off gaps were filled using the approach developed by Maxwell et al. (2007). Landsat and Sentinel-2A data (10-20 m resolution for multispectral bands) were first calibrated radiometrically, then converted into a surface reflectance using the ATCOR-2 code (Richter and Schläpfer, 2014), with image-based visibility estimation (Kaufman et al., 1997), compensating for the adjacency effect (1 km radius). Homologous spectral bands from the multi-sensor dataset were retained for further processing by selecting the best-matching Landsat and Sentinel-2A bands covering the ranges of the four SPOT5 bands (Table 2).

Table 2. Homologous spectral bands used to obtain consistent reflectance time series for each sensor and satellite employed.

		Corresponding spectral bands for each sensor (acronym, satellite)			
Spectral range	**Symbol**	**Enhanced thematic mapper + (ETM+, Landsat 7)**	**Operational land imager (OLI, Landsat 8)**	**High-resolution geometric inst. (HRG, SPOT5)**	**Multi-spectral instrument (MSI, Sentinel-2A)**
visible reflectance – green (Green)	ρ_{Green}	Band 2	Band 3	Band 1	Band 3
visible reflectance – red (Red)	ρ_{Red}	Band 3	Band 4	Band 2	Band 4
near-infrared reflectance (NIR)	ρ_{NIR}	Band 4	Band 5	Band 3	Band 8
shortwave infrared reflectance (SWIR1)	ρ_{SWIR1}	Band 5	Band 7	Band 4	Band 11

The geometric and radiometric quality of the multi-sensor satellite data was assessed to ensure the dataset met the usual requirements for the inter-sensor geometric consistency and radiometric accuracy of spectral reflectance data derived from different medium-resolution platforms (SPOT5, Landsat 7/8, Sentinel-2A). Details are provided in the Supplementary Material.

3.2.Modelling the macrophyte LAI

Following the approach taken by Villa et al. (2017), macrophyte LAI maps were derived from the satellite data by semi-empirical regression modelling based on spectral indices (SIs). Macrophyte LAI data collected *in situ* during the 2015 growing season at the Mantua lakes (representing homogeneous macrophyte plots about 10 x 10 m in size) were divided into two subsets (Table S1), using two thirds of

Received 3 October 2017, Accepted 27 June 2018, Available online 11 July 2018 (**embargo expires 11 July 2020**)

Published version available at: https://doi.org/10.1016/j.rse.2018.06.048

the material for calibrating purposes (30 samples), and the other third for validation (15 samples) of the semi-empirical LAI model implemented.

A set of ten SIs sensitive to the morphology of the canopy of vegetation, and based on broadband surface reflectance in four spectral ranges (Green, Red, NIR, and SWIR1; see Table 2) matching the SPOT5 bands, was tested (Table 3, including related references). The four-range broadband reflectance spectra for each macrophyte plot sampled at the Mantua lakes were derived from the SPOT5 data (at a resolution of 10 m per pixel) acquired within 5 days of the *in situ* data collection. The SPOT5 spectra were extracted from 3 x 3 pixel windows centered on the site of *in situ* sampling, retaining the pixel with the densest vegetation cover as a matchup sample (Villa et al., 2017).

Reflectance spectra for all matchup samples (N=45) were then used to derive the SIs listed in Table 3, for both the calibration and the validation sets. The coefficient of determination (R^2) between the *in situ* macrophyte LAI and the SPOT5-derived SIs for the calibration set (N = 30; Table S1) was used as an indicator of the goodness of fit, and this parameter was adopted to select the best SIs for LAI modelling purposes by means of a linear regression (see last column of Table 3).

The performance of the LAI model was judged in terms of mean absolute error (MAE), mean absolute percentage error (MAPE), and R^2, calculated over the separate validation set (N = 15; Table S1).

Table 3. Spectral indices tested, including index formulas, references and R^2 with macrophyte LAI for the calibration set.

Name	Acronym	Formula	Reference	R^2 *vs.* LAI
Enhanced Vegetation Index 2	EVI2	$2.4\frac{\rho_{NIR}-\rho_{Red}}{\rho_{NIR}+\rho_{Red}+1}$	Jiang et al., 2008	0.889
Modified Triangular Vegetation Index 1	MTVI1	$1.2[1.2(\rho_{NIR}-\rho_{Green})-2.5(\rho_{Red}-\rho_{Green})]$	Haboudane et al., 2004	0.884
Soil-Adjusted Vegetation Index	SAVI	$1.5\frac{\rho_{NIR}-\rho_{Red}}{\rho_{NIR}+\rho_{Red}+0.5}$	Huete, 1988	0.884
Triangular Vegetation Index	TVI	$0.5[120(\rho_{NIR}-\rho_{Green})-200(\rho_{Red}-\rho_{Green})]$	Broge and Leblanc, 2001	0.884
Aerosol-Free Vegetation Index	AFRI	$\rho_{NIR}-0.66\frac{\rho_{SWIR1}}{\rho_{NIR}+0.66\rho_{SWIR1}}$	Karnieli et al., 2001	0.883
Modified Chlorophyll Absorption in Reflectance Index 2	MCARI2	$1.5\frac{2.5(\rho_{NIR}-\rho_{Red})-1.3(\rho_{NIR}-\rho_{Green})}{\sqrt{(2\rho_{NIR}+1)^2-(6\rho_{NIR}-5\sqrt{\rho_{Red}})-0.5}}$	Haboudane et al., 2004	0.880
Green Soil-Adjusted Vegetation Index	GSAVI	$1.5\frac{\rho_{NIR}-\rho_{Green}}{\rho_{NIR}+\rho_{Green}+0.5}$	Tian et al., 2005	0.876
Normalized Difference Vegetation Index	NDVI	$\frac{\rho_{NIR}-\rho_{Red}}{\rho_{NIR}+\rho_{Red}}$	Rouse et al., 1974	0.807
Green Normalized Difference Vegetation Index	GNDVI	$\frac{\rho_{NIR}-\rho_{Green}}{\rho_{NIR}+\rho_{Green}}$	Gitelson and Merzlyak, 1994	0.774
Specific Leaf Area Vegetation Index	SLAVI	$\frac{\rho_{NIR}}{\rho_{Red}+\rho_{SWIR1}}$	Lymburner et al., 2000	0.605

The macrophyte LAI model implemented was then applied to the satellite dataset covering our three study areas (Figure 2). LAI maps were only produced for floating and emergent macrophytes, which were

Received 3 October 2017, Accepted 27 June 2018, Available online 11 July 2018 (**embargo expires 11 July 2020**)

Published version available at: https://doi.org/10.1016/j.rse.2018.06.048

isolated by using a binary raster mask (value = -1) comprising all pixels belonging to the area of the body of water delineated using pre-season data (with a maximum EVI2 < 0.05 in January-March), and covered by vegetation during the growing season (with a maximum EVI2 > 0.10 in April-September).

Areas covered by cloud, identified as pixels with ρ_{Green} > 0.15 surrounded by a 50 m buffer, were masked out of the macrophyte LAI maps (mask value = -1). Then, to homogenize the spatial resolution of the products derived from the multiple sensors with different original resolutions (Landsat, SPOT5 and Sentinel-2A), the macrophyte LAI maps were all resampled at a pixel size of 20 m using bilinear interpolation.

Time series of the macrophyte LAI for the whole year (2015) with a 5-day maximum temporal resolution (the nominal revisit time of the SPOT5 Take5 and the Sentinel-2A/B joint constellation) were prepared by filling dates with missing satellite acquisitions with void layers (NA value = -1). The periods before April and after September were covered using Landsat and Sentinel-2A data, respectively (see Figure 2).

3.3. Metrics of seasonal dynamics

Quantitative descriptors of macrophyte seasonal dynamics were derived with TIMESAT software, using the macrophyte LAI maps as input (Jönsson and Eklundh, 2002; Jönsson and Eklundh, 2004). The following TIMESAT output parameters (called metrics of seasonal dynamics from now on) were considered: the timing of the start of the growing season (SoS, expressed as the day of the year: DOY); the timing of the growth peak of the season (PoS, as the DOY); the timing of the end of the growing season (EoS, as the DOY); the maximum LAI reached during the season (LAI_max, in m^2 m^{-2}); the rate of increase in the LAI during the early growth phase (LAI_growth, in m^2 m^{-2} d^{-1}); and the rate of decrease in the LAI during the senescence phase (LAI_senescence, in m^2 m^{-2} d^{-1}) (Figure 4).

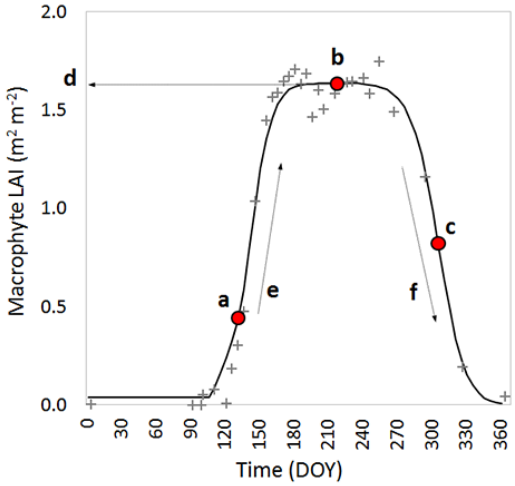

Figure 4. Metrics of seasonal dynamics derived from macrophyte LAI time series using TIMESAT: (a) SoS, (b) PoS, (c) EoS, (d) LAI_max, (e) LAI_growth, (f) LAI_senescence. The example concerns a *Nelumbo nucifera* bed in the Mantua lakes system (45°09'40''N, 10°46'30''E). Grey crosses represent LAI derived from satellite time series, and the black line is the fitted asymmetric Gaussian curve. Adapted from Eklundh and Jönsson (2015).

Received 3 October 2017, Accepted 27 June 2018, Available online 11 July 2018 (**embargo expires 11 July 2020**)

Published version available at: https://doi.org/10.1016/j.rse.2018.06.048

TIMESAT was run without any spike filtering, setting the number of iterations for the envelope to one. The chosen curve fitting method was based on Asymmetric Gaussian curves because it has proved less sensitive to noise and incompleteness of input time series (Gao et al., 2008; Tan et al., 2011). Based on our observations, the start of the growth season coincided with when the macrophytes exceeded 25% of the peak LAI (i.e. 0.25 of the fitted curve amplitude, before the PoS). The end of the season was flagged when the macrophyte LAI decreased to below 50% of the peak value, during the senescent period (i.e. 0.50 of the fitted curve amplitude, after the PoS). For further details on TIMESAT requirements, capabilities and outputs, the reader is referred to the software manual (Eklundh and Jönsson, 2015).

3.4. Influence of input variables on macrophyte phenology estimation

The influence of certain characteristics of the time series data used as input on the resulting macrophyte seasonal dynamics was tested by assessing the variability of key phenology metrics - the SoS, PoS, and EoS - when the multi-temporal dataset used as input was modified. In particular, attention was paid to the sensitivity of the SoS, PoS, and EoS to : i) the amount of cloud cover in the time series used as input; ii) the temporal resolution of the time series; and iii) the relative importance of single dates or periods.
This analysis was conducted using the dataset obtained for the Mantua lakes system, supported by field observations made during the 2015 growing season. The SoS, PoS, and EoS derived from the baseline macrophyte LAI time series with a nominal revisit time of 5 days, acquired during the SPOT5 Take5 experiment (named Mantua_5d from now on, see Table 4), was compared with the same seasonal metrics calculated when the input for TIMESAT was varied as described below. The comparison was drawn by calculating the differences in the SoS, PoS, and EoS outputs over four selected macrophyte beds with different dominant species, environmental conditions and seasonality features (Figure S3). For this purpose, in terms of the mean absolute difference (MAD), and the span between the minimum and maximum values (Max_span) of the SoS, PoS, and EoS derived from the baseline and modified input datasets.

3.4.1. Influence of cloud cover

To examine the influence of the extent of cloud cover, three modified input datasets were prepared using different thresholds for the maximum amount of cloud cover on each image (Figure 2), and excluding the dates when the baseline datasets indicated a cloud cover exceeding the following thresholds (Table 4): 50% (2 images omitted; Mantua_5d_CC50); 30% (4 images omitted; Mantua_5d_CC30); and 10% (7 images omitted; Mantua_5d_CC10).

3.4.2. Influence of temporal resolution

For the influence of temporal resolution, five modified input datasets were examined, based on 10-day and 15-day revisit times (Table 4) to simulate Sentinel-2A and Landsat series, respectively. Two datasets with

Received 3 October 2017, Accepted 27 June 2018, Available online 11 July 2018 (**embargo expires 11 July 2020**)

Published version available at: https://doi.org/10.1016/j.rse.2018.06.048

a 10-day temporal resolution were obtained by alternately omitting and retaining the dates in the baseline dataset, starting from DOY 2 (Mantua_10d_a), or from DOY 7 (Mantua_10d_b). Three datasets with a 15-day temporal resolution were obtained by omitting two in every three dates in the baseline dataset, starting from DOY 2 (Mantua_15d_a), from DOY 7 (Mantua_15d_b), or from DOY 12 (Mantua_15d_c).

3.4.3. Influence of missing acquisitions

To simulate the influence of data missing from a time series covering a whole year, due to cloud cover, bad weather conditions, or other issues related to the sensor (e.g. stoppage for maintenance, or failed acquisitions), 46 modified input datasets were prepared with 5-day and 15-day revisit times (Table 4). Thirty-one datasets with a nominal 5-day temporal resolution were produced by omitting a single date from the LAI time series with an allowable 50% maximum cloud cover (named Mantua_5d_[1-31], depending on the date omitted). Fifteen datasets with a nominal 15-day temporal resolution were produced by omitting a single date from the resampled LAI time series 'Mantua_15d_b' (named Mantua_15d_b_[1-15], depending on the date omitted).

Table 4. Characteristics of datasets of LAI time series used to investigate the influence of input variables on the estimated macrophyte phenology metrics.

Target	Dataset name	Number of images	Short description
Baseline dataset	Mantua_5d	33	complete LAI time series with 5-day revisit time
Influence of cloud cover	Mantua_5d_CC50	31	modified LAI time series with 50% maximum allowable cloud cover
	Mantua_5d_CC30	29	modified LAI time series with 30% maximum allowable cloud cover
	Mantua_5d_CC10	26	modified LAI time series with 10% maximum allowable cloud cover
Influence of temporal resolution	Mantua_10d_a	20	modified LAI time series with 10-day revisit time (starting from DOY 2)
	Mantua_10d_b	19	modified LAI time series with 10-day revisit time (starting from DOY 7)
	Mantua_15d_a	15	modified LAI time series with 15-day revisit time (starting from DOY 2)
	Mantua_15d_b	15	modified LAI time series with 15-day revisit time (starting from DOY 7)
	Mantua_15d_c	15	modified LAI time series with 15-day revisit time (starting from DOY 12)
Influence of missing acquisitions	Mantua_5d_[1-31]	30	modified LAI time series with 5-day revisit time and single dates omitted: steps [1-31] in Mantua_5d_CC50
	Mantua_15d_b_[1-15]	14	modified LAI time series with 15-day revisit time and single dates omitted: steps [1-15] in Mantua_15d_b

4. Results

4.1. Modelling macrophyte LAI

As EVI2 was the SPOT5-derived SI achieving the highest R^2 with the *in situ* macrophyte LAI for the calibration set ($R^2 = 0.889$, Table 3), it was used to implement the semi-empirical LAI model using linear regression, with equation (1):

Received 3 October 2017, Accepted 27 June 2018, Available online 11 July 2018 (**embargo expires 11 July 2020**)

Published version available at: https://doi.org/10.1016/j.rse.2018.06.048

$$\text{LAI } (\text{m}^2\ \text{m}^{-2}) = 2.015(\text{EVI2}) + 0.048 \text{ Range: } [0.0\text{–}2.0\ \text{m}^2\ \text{m}^{-2}] \quad (1)$$

When the LAI scores measured *in situ* were compared with the output of LAI modelling (Figure 5), the overall error level that emerged was 0.11 m^2 m^{-2} in absolute terms (MAE), for both the calibration and the validation sample sets, and less than 18% in relative terms (MAPE 17.7% and 9.6% for the calibration and validation sets, respectively). Over both sample sets, the model tended to slightly underestimate LAI higher than 1.5-1.6 m^2 m^{-2} (corresponding to mature *N. nucifera* plots), with some mismatching at intermediate LAI values for *T. natans* (overestimating LAI > 1 m^2 m^{-2} by ~20%) and *N. lutea* (underestimating low LAI conditions by 15-25%).

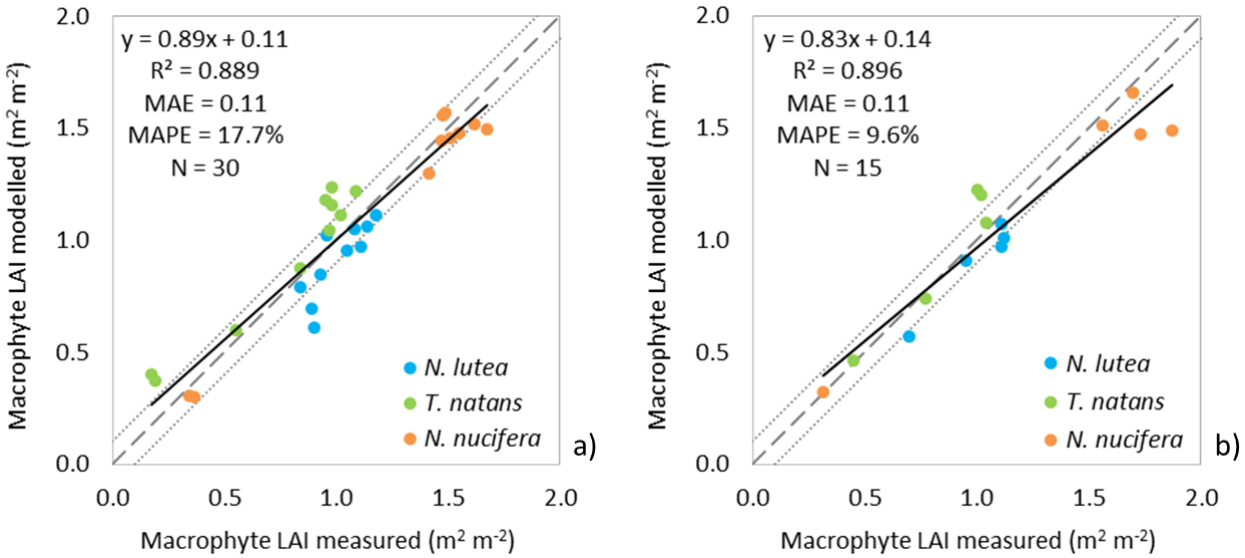

Figure 5. Comparison of macrophyte LAI measured in situ with estimates derived from the EVI2 based semi-empirical linear model implemented (SPOT5 images), over: a) calibration set; b) validation set. Dashed line is the 1:1, dotted lines mark the ±0.1 error line (*N. lutea* = *Nuphar lutea*; *T. natans* = *Trapa natans*; *N. nucifera* = *Nelumbo nucifera*).

4.2.Mapping macrophyte seasonal dynamics

4.2.1. Mantua lakes system

Maps of macrophyte seasonal dynamics derived for the Mantua lakes system are shown in Figure 6. The timing of the start of the growing season differed considerably between the lakes investigated. In particular, *N. nucifera* started to grow at the Superior Lake in mid-May (DOY 125-135), while *T. natans* appeared in mid-May (DOY 130-140) and early June (DOY 155-165) at the Inferior and Middle lakes, respectively (Figure 6a). The peak in seasonal growth (from late July to mid-August) was quite similar for the various species, except for *T. natans* at the Inferior Lake where it was reached already in mid-July (Figure 6b). In fact, the end of the growing season for this latter stand was mid- to late August, while the species disappeared from the Middle Lake about a month later (Figure 6c). The last species to reach

Received 3 October 2017, Accepted 27 June 2018, Available online 11 July 2018 (**embargo expires 11 July 2020**)

Published version available at: https://doi.org/10.1016/j.rse.2018.06.048

senescence was *N. nucifera* (in late October, Figure 6c).

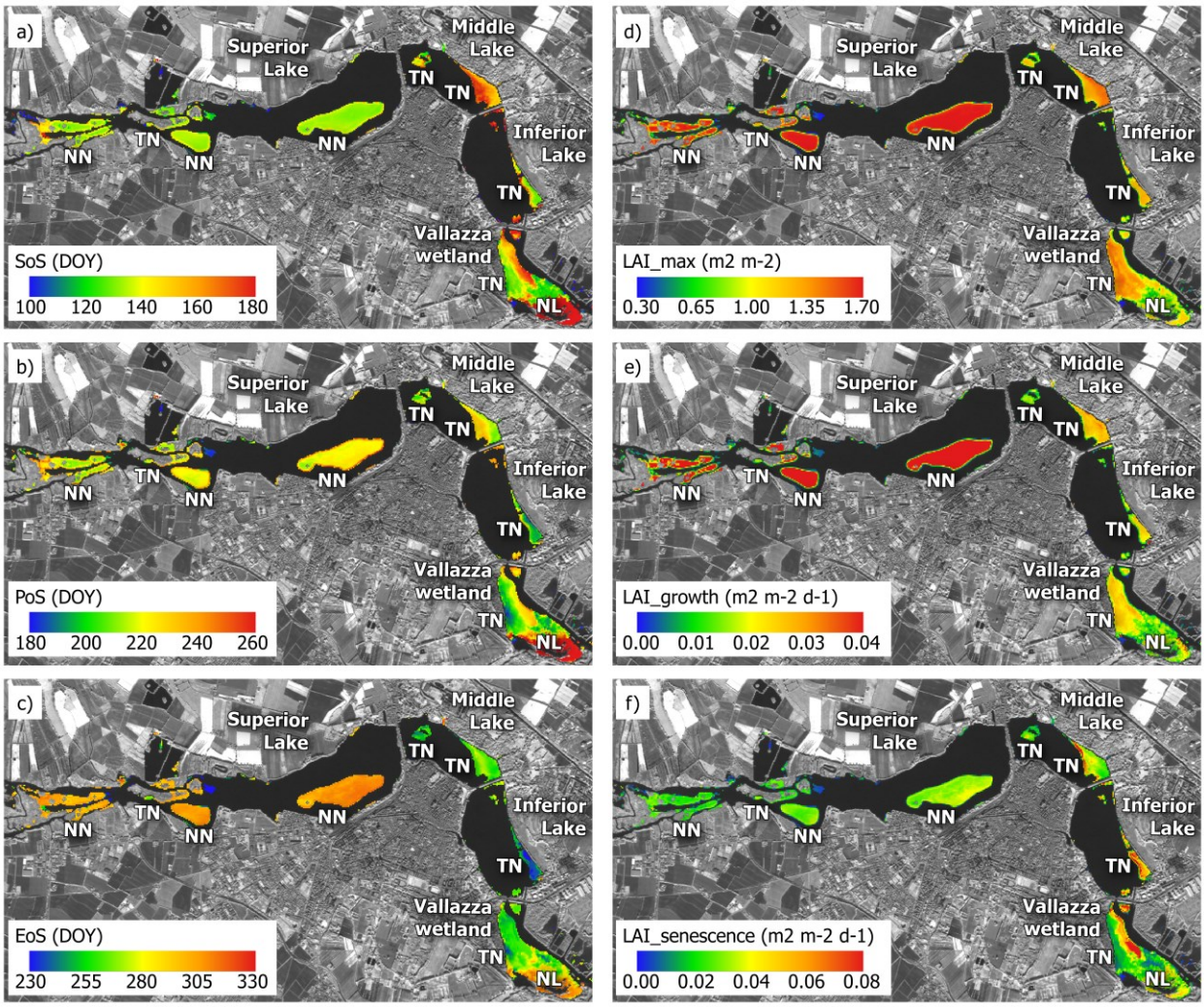

Figure 6. Maps of macrophyte seasonal dynamics for the Mantua lakes system: a) SoS; b) PoS; c) EoS; d) LAI_max; e) LAI_growth; f) LAI_senescence. SoS = start of season, PoS = peak of season, EoS = end of season, LAI_max = maximum LAI value, LAI_growth = rate of increase in LAI during early growth, LAI_senescence = rate of decrease in LAI during senescence (NL = *Nuphar lutea*; TN = *Trapa natans*; NN = *Nelumbo nucifera*).

The LAI scores were higher for *N. nucifera* than for *T. natans* during the early and peak growth phases. During the phase of senescence the LAI decreased at a more homogenous rate, especially in the Middle Lake (Figures 6d, 6e, 6f). For *N. nucifera* and *T. natans* the growing season lasted up to 180 and 120 days, respectively. The maximum LAI for *T. natans* were higher in the Middle Lake than in the Inferior Lake (Figure 6d). The LAI values were much the same for this species in the two lakes during the early growing period (Figure 6e), but during senescence the LAI decreased more quickly in the Inferior than in the Middle Lake (Figure 6f). In the Vallazza wetland, the macrophyte population was composed of several species, including *T. natans* and *N. lutea*, and this was reflected in more patchy dynamics.

Received 3 October 2017, Accepted 27 June 2018, Available online 11 July 2018 (**embargo expires 11 July 2020**)

Published version available at: https://doi.org/10.1016/j.rse.2018.06.048

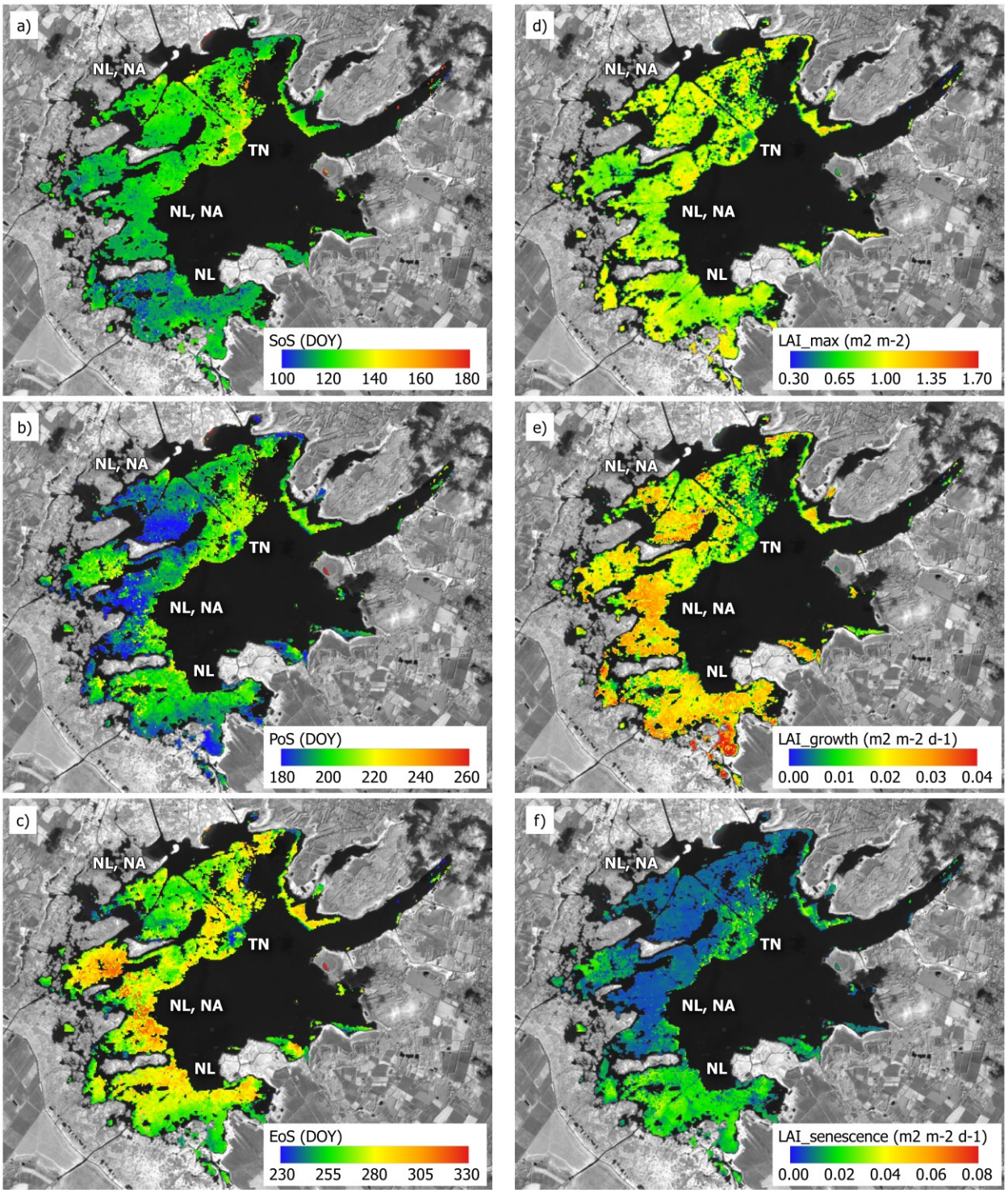

Figure 7. Maps of macrophyte seasonal dynamics for the Lac de Grand-Lieu: a) SoS; b) PoS; c) EoS; d) LAI_max; e) LAI_growth; f) LAI_senescence. Abbreviations are the same as in Figure 6 (NA = *Nymphaea alba*; NL = *Nuphar lutea*; TN = *Trapa natans*).

1.1.1. Lac de Grand-Lieu

The maps of the seasonal dynamics derived for Lac de Grand-Lieu showed a precocious growth of the

Received 3 October 2017, Accepted 27 June 2018, Available online 11 July 2018 (**embargo expires 11 July 2020**)

Published version available at: https://doi.org/10.1016/j.rse.2018.06.048

nymphaeids (*N. alba*, *N. lutea*) to the south of the central part of the lake, where they were growing in sheltered bays where the water was clearer. The species fastest to develop was *T. natans*, identifiable from small blue spots in the middle of the lake in Figures 7b and 7c, showing an early PoS and EoS, around DOY 180 and 230, respectively. The peak LAI mapped for this species in 2015 (0.4-0.6 m^2 m^{-2}) was lower than the value observed in the field in previous years, when *T. natans* beds were denser.

The growth dynamics early in the season shifted in time, depending on the area considered. The areas dominated by *N. lutea*, in the south of the lake where the water level was very low, showed an early peak (DOY 180-185) and a high rate of increase in the LAI. Further analyses are needed, focusing on the balance between *N. alba* and *N. lutea*, to clarify the difference between the nymphaeid beds with similar SoS dates and a moderately high rate of increase in their LAI, but different growth peaks. The areas with the latest EoS (DOY 295 to 330, Figure 7c) can again be attributed to the dominance of *N. alba*, but this species is mixed with *N. lutea* in most parts of the lake, preventing any conclusions from being drawn without first collecting and analyzing further data.

1.1.2. Fundu Mare Island

The seasonal dynamics of the vegetation at Fundu Mare Island in 2015 reflect the changing hydrological conditions throughout the growing season. The colored zones in Figure 8 mark the extent of the area under water when the lakes were maximally inundated (April-June in 2015), before the water levels dropped in summer (Figure 3a).

The maps of macrophyte seasonal dynamics for Fund Mare Island show that, in particular for the aquatic ecosystems, the SoS occurred between DOY 116 and 132 (end of April to early May). In areas with massive willow encroachment, the SoS was sometimes as late as around DOY 180 (late June). The PoS for the floating plants occurred between DOY 195 and 220 (mid- to late July), while it came between DOY 230 and 265 (August to September) for the areas that were no longer under water when the level dropped to around 2 m below its seasonal maximum (by early August, Figure 3a). The EoS likewise showed a clear difference between the deepest parts of the lakes (where it occurred on DOY 250 to 270) and the outer areas that were dry later in the season (where the EoS came after mid-October).

The differences between the plant communities and the duration of their respective inundation are also reflected in the peak LAI scores and their rate of change during growth and senescence. The highest peak LAI (1.35 to 1.65 m^2 m^{-2}) were mapped at the edges of Lake Chiriloaia (especially on the northern, western and southern banks), where terrestrial species grow when water levels are low (in late July). Small patches with a LAI > 1.25 m^2 m^{-2} were found at many sites in both lakes, and can be correlated with the willow-helophyte mosaic (see Figure 3b). The highest rates of change in LAI (Figures 8e and 8f) were observed for deeper areas of the lake covered by floating and floating-leaved species, while the upland areas inhabited by a mosaic of willows and helophytes showed slower rates of growth and senescence.

Received 3 October 2017, Accepted 27 June 2018, Available online 11 July 2018 (**embargo expires 11 July 2020**)

Published version available at: https://doi.org/10.1016/j.rse.2018.06.048

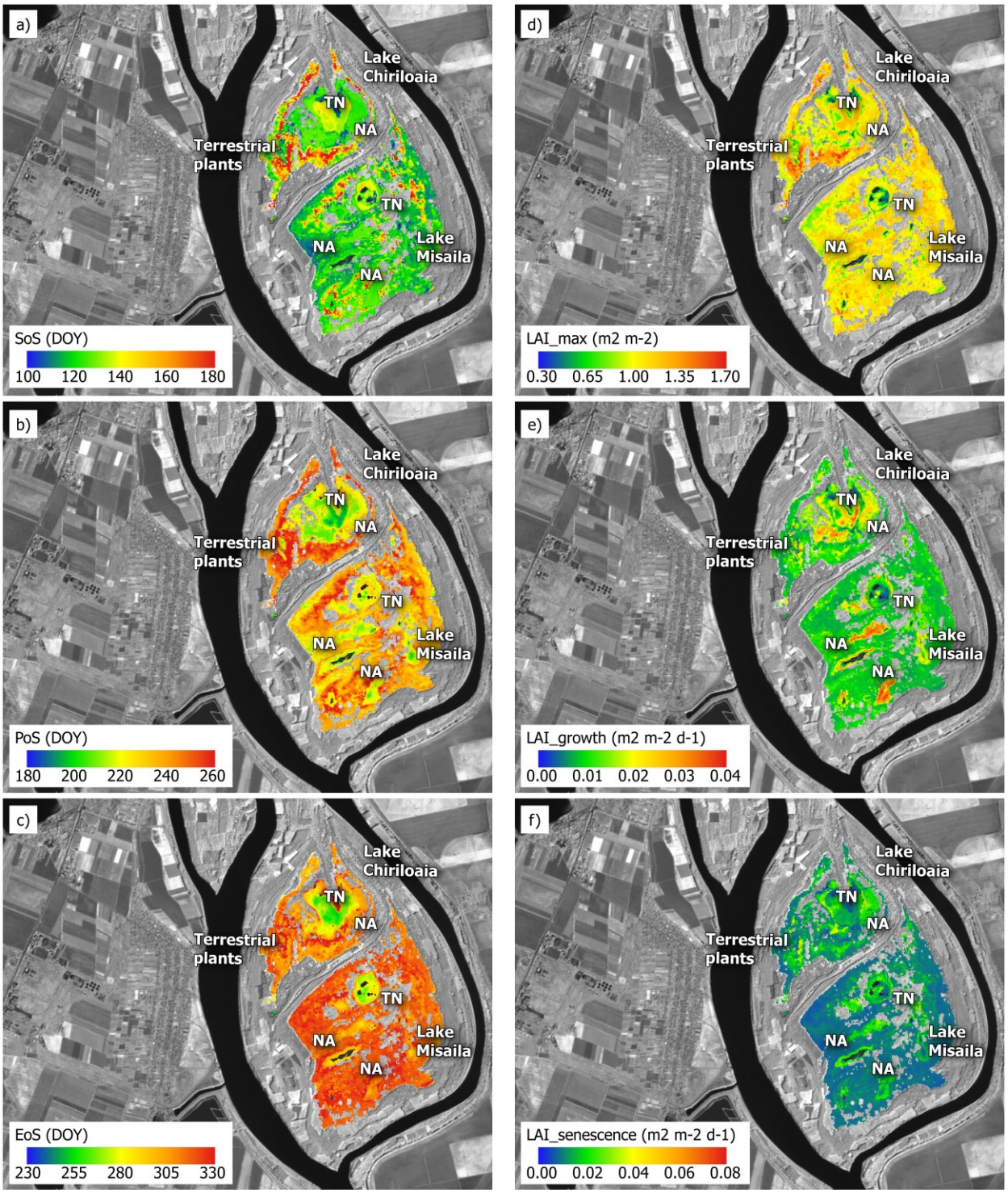

Figure 8. Maps of macrophyte seasonal dynamics for Fundu Mare Island: a) SoS; b) PoS; c) EoS; d) LAI_max; e) LAI_growth; f) LAI_senescence. Abbreviations are the same as in Figure 6 (NA = *Nymphaea alba*; TN = *Trapa natans*).

5.3.Influence of input variables on estimation of macrophyte phenology

5.3.1. Influence of cloud cover

Received 3 October 2017, Accepted 27 June 2018, Available online 11 July 2018 (**embargo expires 11 July 2020**)

Published version available at: https://doi.org/10.1016/j.rse.2018.06.048

As shown in Table 5, the absolute difference in phenology metrics vis-à-vis the baseline under varying cloud cover thresholds (Mantua_5d dataset, see Table 4) was less than 1.5 days, across all macrophyte species investigated. Averaged over all test sample beds, the MAD was lower than 0.8 days, and the Max_span was under 1.9 days. The phenological outputs with no more than 50% cloud cover (Mantua_5d_CC50) showed only slight differences with respect to the baseline (Max_span ≤ 0.34 days), while the results obtained using 30% and 10% maximum cloud cover thresholds diverged a little more, with a Max_span of 1.4 and 1.8 days, respectively. Among the phenology metrics considered, the SoS was more sensitive to changes in the choice of cloud cover (MAD ≤ 0.8 days) than the PoS or EoS (MAD ≤ 0.3 days).

Table 5. Influence of cloud cover threshold for time series input on TIMESAT outputs (SoS, PoS, EoS) for the Mantua lakes system dataset.

		Difference *vs*. baseline (Mantua_5d)		
Dataset*		**ΔSoS (days)**	**ΔPoS (days)**	**ΔEoS (days)**
Mantua_5d_CC10	NNs	0.5	-0.1	-0.6
	TNm	0.7	-0.1	0.1
	TNi	-1.1	0.8	0.0
	NLv	-0.4	0.6	0.0
	MAD	**0.7**	**0.3**	**0.3**
	Max_span	*1.8*	*0.9*	*0.8*
Mantua_5d_CC30	NNs	-1.4	0.3	0.5
	TNm	0.0	0.0	0.1
	TNi	-0.6	0.0	-0.2
	NLv	-0.8	-0.4	0.0
	MAD	**0.8**	**0.2**	**0.3**
	Max_span	*1.4*	*0.7*	*0.7*
Mantua_5d_CC50	NNs	0.0	0.0	0.0
	TNm	0.0	0.0	0.0
	TNi	0.3	0.3	-0.2
	NLv	0.0	0.0	0.0
	MAD	**0.1**	**0.1**	**0.0**
	Max_span	*0.2*	*0.3*	*0.2*

Macrophyte test beds: NNs: *Nelumbo nucifera* (Superior Lake); TNm: *Trapa natans* (Middle Lake); TNi: *Trapa natans* (Inferior Lake); NLv: *Nuphar lutea* (Vallazza wetland).
* see Table 4 for description of datasets.

5.3.2. Influence of temporal resolution

Table 6 shows the differences in phenology metrics vis-à-vis the baseline (Mantua_5d dataset, see Table 4) when the revisit time of the time series used as input was reduced to 10 or 15 days.

When the temporal resolution was degraded to 10 days (as for the nominal Sentinel-2A coverage over Europe and Africa, and for the Sentinel-2A and -2B constellation globally), the absolute differences in SoS, PoS and EoS compared to the baseline, across all macrophyte test beds, never exceeded 3.8 days. Different test beds (i.e. different macrophyte communities) showed a variable sensitivity to this change in temporal resolution. The difference was generally no more than 3.2 days (twice the standard deviation across all test beds). Averaging over all the test beds, the MAD was lower than 1.6 days, and the

Received 3 October 2017, Accepted 27 June 2018, Available online 11 July 2018 (**embargo expires 11 July 2020**)

Published version available at: https://doi.org/10.1016/j.rse.2018.06.048

Max_span was under 2.8 days. Among the phenology metrics considered, the EoS proved more sensitive to the revisit time being extended from 5 to 10 days (MAD = 1.6 days) than the SoS or PoS (MAD ≤ 1.2 days).

Further reducing the temporal resolution to 15 days (near the nominal 16-day revisit time of the Landsat 4-8 satellites collecting data all over the globe since 1982) resulted in absolute differences in the TIMESAT output phenology metrics of up to 5.9 days across all macrophyte test beds. The influence on the phenology metrics varied across the test beds and the species investigated, but was generally no more than 4.8 days difference vis-à-vis the baseline (twice the standard deviation across all test beds). Averaging over all the test beds, the MAD of the 15-day revisit time series did not overpass 2.7 days, while Max_span peaked at 7.3 days. As with the 10-day temporal resolution, the EoS was more sensitive (MAD = 2.7 days) than the SoS or PoS (MAD ≤ 1.8 days).

Table 6. Influence of temporal resolution of the time series used for input on the TIMESAT output metrics (SoS, PoS, EoS) for the Mantua lakes system dataset.

		Difference *vs*. baseline (Mantua_5d)		
Dataset*		**ΔSoS (days)**	**ΔPoS (days)**	**ΔEoS (days)**
Mantua_10d_a	NNs	1.8	-3.8	-3.6
	TNm	-0.3	0.7	2.4
	TNi	-0.7	-0.4	-1.1
	NLv	1.3	1.4	0.2
Mantua_10d_b	NNs	0.9	-0.4	-0.5
	TNm	-2.6	0.5	0.8
	TNi	0.3	-0.1	2.2
	NLv	-0.8	-1.0	-0.5
Mantua_10d	**MAD**	**1.2**	**1.1**	**1.6**
	Max-span	*1.9*	*2.0*	*2.7*
Mantua_15d_a	NNs	1.2	1.7	4.5
	TNm	-2.8	1.3	2.6
	TNi	-0.8	-3.7	-0.9
	NLv	1.0	0.5	3.9
Mantua_15d_b	NNs	-1.2	-4.3	-5.9
	TNm	-2.1	-3.2	-5.3
	TNi	4.0	0.8	-0.1
	NLv	0.3	-0.1	-3.2
Mantua_15d_c	NNs	1.4	-1.3	-1.5
	TNm	-2.0	-0.7	-0.6
	TNi	-1.5	-0.4	0.3
	NLv	-0.7	0.5	-0.2
Mantua_15d	**MAD**	**1.6**	**1.8**	**2.7**
	Max_span	*3.1*	*4.5*	*7.3*

Macrophyte test beds: NNs: *Nelumbo nucifera* (Superior Lake); TNm: *Trapa natans* (Middle Lake); TNi: *Trapa natans* (Inferior Lake); NLv: *Nuphar lutea* (Vallazza wetland).
* see Table 4 for a description of the datasets.

5.3.3. Influence of missing acquisitions

Received 3 October 2017, Accepted 27 June 2018, Available online 11 July 2018 (**embargo expires 11 July 2020**)

Published version available at: https://doi.org/10.1016/j.rse.2018.06.048

Based on the phenology metrics derived from the full Mantua lakes system dataset with a 5-day temporal resolution (Figures 6a-c), five seasonal periods were identified, namely: i) pre-season (DOY < 100); ii) early season, comprising the SoS dates for most of the macrophytes (100 < DOY < 180); iii) full season, when the vegetative and reproductive phase of the macrophyte communities investigated peaked (180 < DOY < 250); iv) late season, after plants had reached maturity and senescence set in (250 < DOY < 320); and v) post-season (DOY > 320). These five seasonal periods were considered in interpreting our findings concerning the influence of missing acquisitions.

With a 5-day revisit time (Figure 9a), the EoS was the parameter most sensitive to a single date being omitted from the time series, with a MAD vis-à-vis the Mantua_5d_CC50 dataset (see Table 4) reaching 3.5 days, while the SoS and PoS were less influenced by missing dates (MAD of 1.7 and 0.8, respectively). The sensitivity of the phenology metrics to this factor was most pronounced for the NNs test bed (populated by *N. nucifera*), with a maximum difference of up to 8.3 days for the EoS, and up to 4.2 days for the PoS, by comparison with the full dataset (when the acquisition on DOY 297 was omitted from the time series). The other macrophyte test beds, populated by *T. natans* and *N. lutea*, were less sensitive to missing acquisitions, with maximum differences vis-à-vis the baseline of less than 1.5 days. The key periods for capturing phenology from satellite LAI time series effectively are therefore early in the season (April-May) for estimating the SoS, late in the season (September-October) for estimating the PoS and EoS, and at or after the end of the season (October-November) for estimating the EoS.

With a 15-day revisit time (Figure 9b), the results were generally consistent with the findings obtained with a 5-day revisit time, albeit with wider ranges of the scores. The SoS and EoS were the parameters most sensitive to the omission of a single date, with a MAD vis-à-vis the Mantua_15d_b dataset (see Table 4) of around 2.7 days, while for the PoS the MAD was 1.5 days. Sensitivity to missing acquisitions was, here again, most pronounced for the NNs test bed, with a maximum difference vis-à-vis the full dataset of up to 5.1 days for the SoS, and up to 5.4 days for the EoS. The phenology metrics of TNm test bed (populated by *T. natans*) proved highly sensitive to missing acquisitions too, with differences of up to 7.9 days for the EoS if dates at or after the end of the season were omitted from the time series. The phenology metrics for TNi (also populated by *T. natans*) were less sensitive to this change (maximum difference of 4.2 days), and those for NLv (populated by *N. lutea*) were even less so (< 2 days). At seasonal level, the key periods with a 15-day temporal resolution were the same as for a 5-day revisit time.

Received 3 October 2017, Accepted 27 June 2018, Available online 11 July 2018 (**embargo expires 11 July 2020**)

Published version available at: https://doi.org/10.1016/j.rse.2018.06.048

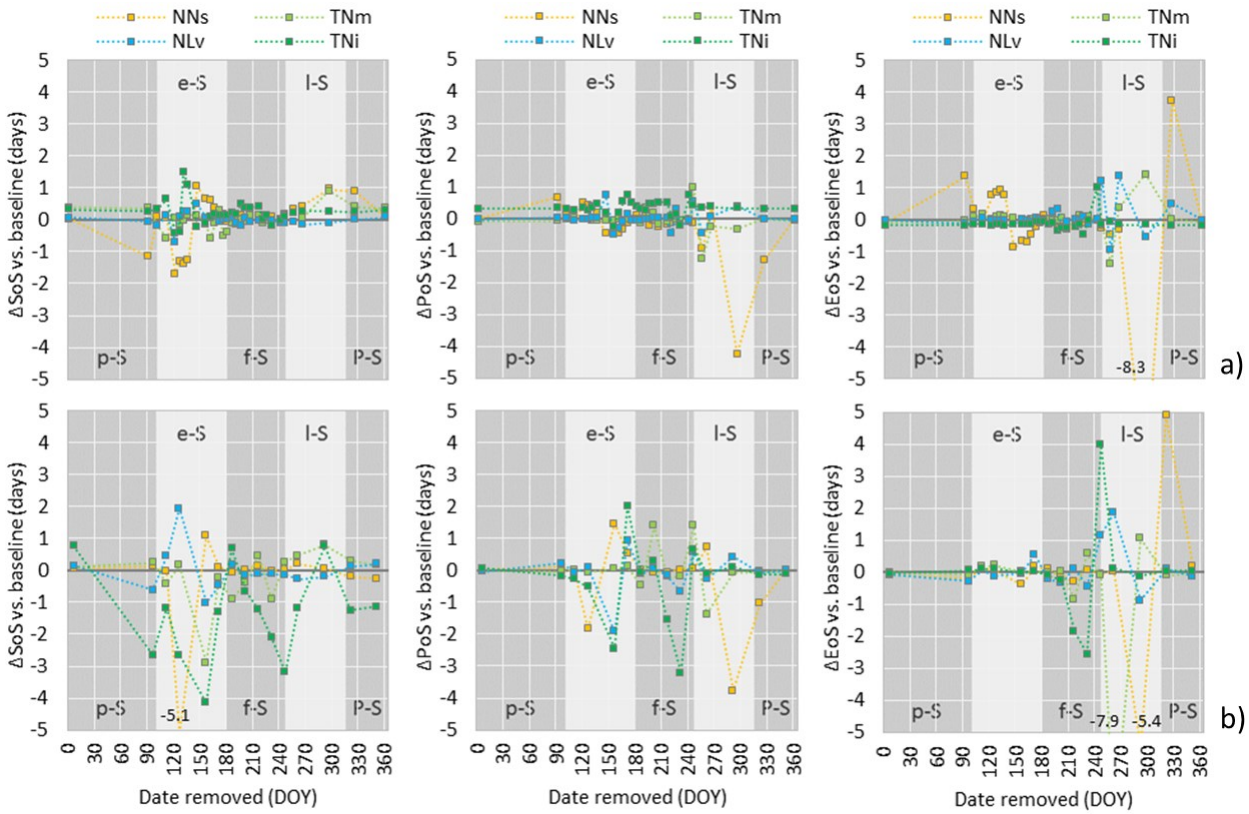

Figure 9. Influence of omitting dates in the time series used as input on the TIMESAT output metrics (SoS, PoS, EoS) for the Mantua lakes system with: a) a 5-day temporal resolution; and b) a 15-day temporal resolution. Seasonal periods are identified by different shades of grey background: p-S: pre-season; e-S: early season; f-S: full season; l-S: late season; P-S: post-season. Macrophyte test beds: NNs: *Nelumbo nucifera* (Superior Lake); TNm: *Trapa natans* (Middle Lake); TNi: *Trapa natans* (Inferior Lake); NLv: *Nuphar lutea* (Vallazza wetland).

6. Discussion

6.1.Macrophyte LAI mapping from satellite data

Satellite data coming from different medium-resolution platforms (SPOT5, Landsat 7/8, Sentinel-2A) can be integrated into consistent time series of surface spectral reflectance with a temporal misregistration of less than 0.3 pixels (Dai and Khorram, 1998). The radiometric mismatch across sensors remains within acceptable levels, i.e. a relative MAE < 0.04 between SPOT5 and Landsat 8 or Sentinel-2A data, and an absolute MAE < 0.07 compared to *in situ* spectra (Figure S2). Compared to EVI2 derived from SPOT5 bands, both Landsat 8 and Sentinel-2A tend to score around 30% higher on the high-end values (Figure S1). This is probably due to differences in the atmospheric correction algorithms used for the two types of data (MACCS for SPOT5 and ATCOR for Landsat and Sentinel-2), which implies that the macrophyte LAI maps may be slightly overestimated in the temporal range not covered by SPOT5 Take5 dataset. The period in question (before April and after September) was largely outside the growing season for macrophytes in temperate areas, however, so the effect on the TIMESAT-derived phenology metrics was

Received 3 October 2017, Accepted 27 June 2018, Available online 11 July 2018 (**embargo expires 11 July 2020**)

Published version available at: https://doi.org/10.1016/j.rse.2018.06.048

judged to have been minimal, with a negligible influence on the results of this study.

LAI for target macrophyte species (floating, floating-leaved, emergent) was reliably estimated using the semi-empirical regression model based on EVI2 (the best-performing spectral index): the MAE for the independent validation data was 0.11 m^2 m^{-2}, with a tendency for underestimation due to index saturation in canopy closure conditions, which for the plant species and groups investigated can occur at LAI > 1.5 m^2 m^{-2}. These results, obtained with experimental data covering a whole growing season, demonstrate that macrophyte LAI mapping based on spectral indices is feasible, with acceptable errors. The concept, already well established in the scientific literature for terrestrial vegetation, has only recently been developed on a sound basis for aquatic vegetation too (see Villa et al., 2014). The present work corroborates and adds to the findings published by Villa et al. (2017), by extending their potential application in macrophyte morphology mapping to broadband multispectral platforms.

The LAI model was calibrated (and validated) with reference to *in situ* measurements collected with the same spatial resolution (10 m grid) as the SPOT5 data. This approach is consistent with good practice and the protocols (e.g. Weiss et al., 2004; Hufkens et al., 2008) for recording the biophysical characteristics of vegetation for linking with medium-high resolution (≤ 30 m pixel) remotely sensed data. Garrigues et al. (2006) wrote that such practices are based on the assumption of a homogeneous vegetation cover at this scale, an assumption that was verified by direct observation of the macrophyte beds surveyed for the present study.

This work focused on floating and emergent forms of aquatic vegetation. The optical spectral response of submerged macrophytes is largely determined by the properties of the water column above them, and the use of remotely sensed spectral reflectance to estimate their biophysical parameters is virtually unfeasible (e.g. Hunter et al., 2010, Villa et al., 2015) in systems with water as turbid, as in the majority of shallow lakes hosting aquatic plant communities in abundance. Even where submerged and floating/emergent species coexist and turbidity is low, the high absorption of near-infrared light by clear water makes the influence of submerged macrophytes on the SIs tested (and therefore on our estimates of macrophyte LAI) practically negligible (e.g. Malthus, 2017).

6.2.Macrophyte seasonal dynamics in the study areas

The maps of seasonal dynamics derived using TIMESAT, with macrophyte LAI time series as input, showed differences in both spatial and temporal patterns across the three study areas, all temperate shallow water ecosystems populated by much the same macrophyte species.

In our study areas, the growing season of the nymphaeids (mainly *N. lutea* and *N. alba*) took place 10-30 days later in Fundu Mare Island than in the Mantua lakes system or Lac de Grand-Lieu. This was possibly due to the water level fluctuations observed in the Romanian wetland (Figure 3a), where the peak LAI for floating-leaved plant communities was higher than 1.1 m^2 m^{-2} due to the interference of willow

Received 3 October 2017, Accepted 27 June 2018, Available online 11 July 2018 (**embargo expires 11 July 2020**)

Published version available at: https://doi.org/10.1016/j.rse.2018.06.048

encroaching on the *N. alba* beds (Figure 8d). In the Lac de Grand-Lieu, the seasonal dynamics of the nymphaeids might also influence our interpretation of the maps. *N. alba* may have a bimodal growth, with a first peak in biomass in spring and a second late in summer, or it may have just a single growth peak (Paillisson and Marion, 2006), depending on the year, and probably varying locally within the lake. The Mantua lakes system, where nymphaeids cover only a small area (< 6% of macrophyte surface) had the shortest growing season and the slowest rate of increase in LAI for these plants of all three sites investigated (Figure 6a-b and 6e).

Water chestnut (*T. natans*), the other species common to all three study areas, showed the highest intra-site variability in phenology metrics (SoS, PoS, EoS) in the Mantua lakes system, where different sub-systems are associated with a spatially heterogeneous phenology. This goes to show that *T. natans* is capable of adapting to different environmental conditions and trophic levels, thus becoming dominant everywhere except in the Superior Lake, and accounting for almost 50% of the total macrophyte area. On average, this species starts growing later in the Mantua lakes system and reaches peak LAI values higher than 1.20 m^2 m^{-2} (Figure 6d). Such high scores are anomalous for a floating plant, and are due to *T. natans* being mixed with duckweed (such as *Lemna* ssp., *Spirodela polyrhiza*), in the Middle and Inferior lakes in high summer (July and August), with a consequent increase in the total leaf area per unit of surface area.

In the Lac de Grand-Lieu, where *T. natans* covers only a small part (< 5%) of the total macrophyte area, and is outcompeted by nymphaeids, the growing season peaks and ends earlier than at the other two sites (Figure 7b-c), and the density reached by the plant is by far the lowest, with a maximum LAI ~ 0.5-0.6 m^2 m^{-2} (Figure 7d). The species has been in decline for the last forty years at the Lac de Grand-Lieu, but the hydro-meteorological conditions in the spring of 2015 may have exacerbated the trend: a late flood at the beginning of May raised the lake level by 40 cm in 5 days, negatively affecting *T. natans* germination and growth.

The allochthonous sacred lotus (*N. nucifera*) is only to be found in the Mantua lakes system, where it was introduced in 1921. The maps of its seasonal dynamics clearly show the distinctly invasive traits of this species, characterized by rapid growth (0.03-0.05 m^2 m^{-2} d^{-1}, from May to June; Figure 6e), persistence (EoS in October-November; Figure 6c), and high density and coverage (LAI up to 1.7 m^2 m^{-2}; Figure 6d). These characteristics can easily explain how the autochthonous species (*T. natans* and *N. lutea*) have been outcompeted by *N. nucifera* over the last century in the Mantua lakes system. This has led to a situation where sacred lotus almost completely dominates the Superior Lake, accounting for up to 45% of the total macrophyte area, and needs to be cut back on a yearly basis (Villa et al., 2017). This is a crucial issue, considering the very large number of allochthonous species spreading in aquatic ecosystems, especially in temperate regions (Hussner, 2012; Bolpagni et al., 2013). They have become one of the most critical

Received 3 October 2017, Accepted 27 June 2018, Available online 11 July 2018 (**embargo expires 11 July 2020**)

Published version available at: https://doi.org/10.1016/j.rse.2018.06.048

factors for the survival of autochthonous aquatic species and habitats (Gallardo et al., 2016).
In this study, the timing of the start of the season was defined as the moment when the macrophytes exceeded 25% of their peak LAI, based on observation of target macrophyte species. This may differ, however, where willow canopy has encroached widely - as seen at Fundu Mare Island. Young *Salix* spp., partly inundated during the spring, developed only later in the season, depending on the dropping water levels, consequently affecting the LAI mapped for macrophyte patches subject to their encroachment, and also influencing the interpretation of some maps of seasonal dynamics (Figure 8).
The composition, structure and vigor of riparian vegetation respond rapidly to changes in hydrological regime (e.g. Merritt et al., 2010; Johnson, 2000; Loheide and Booth, 2011). This study showed that the TIMESAT-derived metrics of seasonal dynamics, and PoS and EoS in particular, could be correlated with specific types of plant community. Vegetation zoning in floodplains like Fundu Mare Island is closely related to the duration of flooding and the mean summer water level (Ellenberg, 1996).
The availability of medium-resolution satellite data offers new opportunities for studying ongoing changes in vegetation cover and monitoring its anomalies, such as the encroachment of willows in areas previously mapped as aquatic habitats. Describing the seasonal dynamics of vegetation in terms of LAI, which can be used to parametrize the flow resistance of floodplain vegetation (Aberle and Järvelä, 2013), may also support the application of hydrodynamic models of flow and sediment transport in complex riparian environments.

6.3. Influence of satellite data variables on phenology metrics

It is important to assess the impact of the characteristics of satellite data on TIMESAT-derived macrophyte seasonal dynamics in order to delineate operational requirements, as well as to quantify the error levels to be expected when the resolution of time series used as input is reduced due to cloud cover, sensor revisit times are longer, or acquisitions are missing. Although it was based exclusively on empirical data for the Mantua lakes system, our assessment provides a first, quantitative account of how sensitive key phenology metrics of floating and emergent aquatic vegetation may be to cloud cover on a given date, temporal resolution, and missing acquisitions within input time series, thanks to the temporal resolution afforded by the SPOT5 Take5 experiment (which anticipated the operational features of Sentinel-2 constellation). For datasets obtained with a 5-day revisit time, the effect of setting different cloud cover thresholds was limited to under 2 days for estimating the SoS, and even less for the PoS and EoS. The temporal resolution proved most influential, reaching maximum differences in EoS estimation of 2.8 and 7.4 days, respectively, when the revisit time for the input time series changed from the nominal 5 days to 10 and 15 days (as in Landsat series). The difference was less severe for the SoS and PoS, for which the estimation bias could reach 1.8 and 3.1 days, respectively. Based on these results, data acquired consistently all over the globe with Landsat since 1982 could be used retrospectively to map the

Received 3 October 2017, Accepted 27 June 2018, Available online 11 July 2018 (**embargo expires 11 July 2020**)

Published version available at: https://doi.org/10.1016/j.rse.2018.06.048

phenology metrics of macrophytes at a 30 m spatial resolution, with an error level of around 2-3 days for the SoS and PoS.

When the influence of missing acquisitions (due to cloud cover, for instance) was analyzed, the EoS was again the most sensitive parameter, with estimation bias of 3.5 days an average, and 8.3 days at most, when satellite images were missing late in the season (from mid-September to mid-November). The differences for the SoS and PoS were limited to 2 days and 5 days, respectively, at most. Bias scores were higher for *N. nucifera*, while differences in phenology metrics for *T. natans* and *N. lutea* were generally lower (< 1.5 days).

7. Conclusions

Our findings demonstrate that dense time series of different medium-resolution satellite data (i.e. Landsat, SPOT, Sentinel-2) can be integrated to provide consistent LAI maps of macrophytes and their seasonal dynamics, although some criticalities remain concerning atmospheric correction with different algorithms, and the correspondence between TIMESAT-derived metrics and actual phenological phases of different plant species. For the first time, the feasibility of reliably estimating macrophyte LAI with operational Earth Observation data was demonstrated, also assessing the sensitivity of key phenology metrics to cloud cover thresholds, revisit times, and missing acquisitions in the satellite time series used as input.

Using satellite data to map macrophyte dynamics quantitatively on a local-to-regional scale offers new opportunities for monitoring restoration and conservation action in shallow aquatic ecosystems, elucidating the effects of measures to influence the hydrological conditions as well as the rapid changes characteristic of intra- and inter-seasonal macrophyte dynamics.

The results reported here also confirm the efficacy of remote sensing techniques in investigating the factors driving the potential establishment of allochthonous species, and the competition between autochthonous and allochthonous species in particular.

Acknowledgements

This study received funding from the European Community's 7th Framework Programme, under project INFORM [grant no. 606865]. SPOT5 data were acquired within the framework of the SPOT5 (Take5) initiative, sponsored by the CNES and the ESA, and the time series covering the Mantua lakes system was proposed as part of the MacroSentinel project [ESA project ID 29146].

Monitoring of the floating macrophytes in Lac de Grand-Lieu was supported by the Regional Directorate for the Environment (DREAL) of Pays de la Loire, the Regional Council of Pays de la Loire, and the Loire-Atlantique Federation of Hunters.

The investigations at Fundu Mare Island were funded by the European Economic Area (EEA) project

Received 3 October 2017, Accepted 27 June 2018, Available online 11 July 2018 (**embargo expires 11 July 2020**)

Published version available at: https://doi.org/10.1016/j.rse.2018.06.048

"Restoration of the aquatic and terrestrial ecosystems of Fundu Mare Island" [grant no. RO02-0008] with financial contributions from Norway and Romania, and with the support of the Natural Park Administration of the Small Wetland of Braila.

The authors thank Ilaria Cazzaniga (CNR-IREA) for her help during fieldwork on the Mantua lakes system and Frances Coburn for English language editing.

References

Aberle J, Järvelä J (2013) Flow resistance of emergent rigid and flexible floodplain vegetation. Journal of Hydraulic Research, 51, 33–45.

Alahuhta, J., Heino, J., & Luoto, M. (2011). Climate change and the future distributions of aquatic macrophytes across boreal catchments. Journal of Biogeography, 38(2), 383-393.

Bolpagni, R., Bartoli, M., & Viaroli, P. (2013). Species and functional plant diversity in a heavily impacted riverscape: Implications for threatened hydro-hygrophilous flora conservation. Limnologica, 43, 230-238.

Bolpagni, R., Bresciani, M., Laini, A., Pinardi, M., Matta, E., Ampe, E.M., Giardino, C., Viaroli, P., & Bartoli M. (2014). Remote sensing of phytoplankton-macrophyte coexistence in shallow hypereutrophic fluvial lakes. Hydrobiologia 737: 67-76.

Broge, N. H., & Leblanc, E. (2001). Comparing prediction power and stability of broadband and hyperspectral vegetation indices for estimation of green leaf area index and canopy chlorophyll density. Remote Sensing of Environment, 76(2), 156-172.

Cleland, E. E., Chuine, I., Menzel, A., Mooney, H. A., & Schwartz, M. D. (2007). Shifting plant phenology in response to global change. Trends in Ecology & Evolution, 22(7), 357-365.

Dai, X., & Khorram, S. (1998). The effects of image misregistration on the accuracy of remotely sensed change detection. IEEE Transactions on Geoscience and Remote Sensing, 36(5), 1566-1577.

Drusch, M., Del Bello, U., Carlier, S., Colin, O., Fernandez, V., Gascon, F., Hoersch, B., Isola, C., Laberinti, P., Martimort, P., Meygret, A., Spoto, F., Sy, O., Marchese, F. & Bargellini, P. (2012). Sentinel-2: ESA's optical high-resolution mission for GMES operational services. Remote Sensing of Environment, 120, 25-36.

Eklundh, L. & Jönsson, P. (2015). Timesat 3.2 Software Manual, Lund and Malmö University, Sweden. http://web.nateko.lu.se/timesat/docs/TIMESAT32_software_manual.pdf

Ellenberg, H. 1996. Vegetation Mitteleuropas mit den Alpen. 5. Auflage. Ulmer Verlag.

Fensholt, R., Horion, S., Tagesson, T., Ehammer, A., Grogan, K., Tian, F., Huber, S., Verbesselt, J., Prince, S.D., Tucker, C.J. & Rasmussen, K., 2015. Assessment of vegetation trends in drylands from time series of Earth observation data. In Remote Sensing Time Series, Springer International Publishing, 159-182.

Fisher, J. I., & Mustard, J. F. (2007). Cross-scalar satellite phenology from ground, Landsat, and MODIS data. Remote Sensing of Environment, 109(3), 261-273.

Fisher, J. I., Richardson, A. D., & Mustard, J. F. (2007). Phenology model from surface meteorology does not capture satellite-based greenup estimations. Global Change Biology, 13(3), 707-721.

Gao, F., Morisette, J. T., Wolfe, R. E., Ederer, G., Pedelty, J., Masuoka, E., Myneni, R., Tan, B. & Nightingale, J. (2008). An algorithm to produce temporally and spatially continuous MODIS-LAI time series. IEEE Geoscience and Remote Sensing Letters, 5(1), 60-64.

Gallardo, B., Clavero, M., Sánchez, M. I., & Vilà, M. (2016). Global ecological impacts of invasive species in aquatic ecosystems. Global Change Biology, 22(1), 151-163.

Garrigues, S., Allard, D., Baret, F., & Weiss, M. (2006). Influence of landscape spatial heterogeneity on the non-linear estimation of leaf area index from moderate spatial resolution remote sensing data. Remote Sensing of Environment, 105(4), 286-298.

Gillier J.M. & Reeber S. (2016). Suivi spatial de la zone centrale du Lac de Grand-Lieu en 2015. DREAL Pays de la Loire, Région Pays de la Loire, Syndicat de Bassin Versant de Grand-Lieu, SNPN, Fédération Départementale des Chasseurs de Loire-Atlantique. pp. 24.

Gitelson, A., & Merzlyak, M. N. (1994). Quantitative estimation of chlorophyll-a using reflectance spectra: Experiments with autumn chestnut and maple leaves. Journal of Photochemistry and Photobiology B: Biology, 22(3), 247-252.

Haboudane, D., Miller, J. R., Pattey, E., Zarco-Tejada, P. J., & Strachan, I. B. (2004). Hyperspectral vegetation

Received 3 October 2017, Accepted 27 June 2018, Available online 11 July 2018 (**embargo expires 11 July 2020**)

Published version available at: https://doi.org/10.1016/j.rse.2018.06.048

indices and novel algorithms for predicting green LAI of crop canopies: Modeling and validation in the context of precision agriculture. Remote Sensing of Environment, 90(3), 337-352.

Hagolle, O., Huc, M., Villa Pascual, D., & Dedieu, G. (2015). A multi-temporal and multi-spectral method to estimate aerosol optical thickness over land, for the atmospheric correction of Formosat-2, Landsat, Venμs and Sentinel-2 images. Remote Sensing, 7(3), 2668-2691.

Haury J., Noël F., Bozec M., Coudreuse J., Guil J., Marrel G., Maisonneuve J.L. & Damien J.P. (2011). Importance of Ludwigia grandiora as invasive weed on meadows and pastures in Western France. 3rd International Symposium on Weeds and Invasive Plants, Oct 2011, Ascona (CH), Switzerland.

Hestir, E. L., Brando, V. E., Bresciani, M., Giardino, C., Matta, E., Villa, P., & Dekker, A. G. (2015). Measuring freshwater aquatic ecosystems: The need for a hyperspectral global mapping satellite mission. Remote Sensing of Environment, 167, 181-195.

Huete, A. R. (1988). A soil-adjusted vegetation index (SAVI). Remote Sensing of Environment, 25(3), 295-309.

Hufkens, K., Bogaert, J., Dong, Q. H., Lu, L., Huang, C. L., Ma, M. G., Che, T., Li, X., Veroustraete, F. & Ceulemans, R. (2008). Impacts and uncertainties of upscaling of remote-sensing data validation for a semi-arid woodland. Journal of Arid Environments, 72(8), 1490-1505.

Hunter, P. D., Gilvear, D. J., Tyler, A. N., Willby, N. J., & Kelly, A. (2010). Mapping macrophytic vegetation in shallow lakes using the Compact Airborne Spectrographic Imager (CASI). Aquatic Conservation: Marine and Freshwater Ecosystems, 20(7), 717-727.

Hussner, A. (2012). Alien aquatic plant species in European countries. Weed Research, 52(4), 297-306.

Jenkins, J. P., Braswell, B. H., Frolking, S. E., & Aber, J. D. (2002). Detecting and predicting spatial and interannual patterns of temperate forest springtime phenology in the eastern US. Geophysical Research Letters, 29(24).

Jiang, Z., Huete, A. R., Didan, K., & Miura, T. (2008). Development of a two-band enhanced vegetation index without a blue band. Remote Sensing of Environment, 112(10), 3833-3845.

Johnson, W.C. 2000. Tree recruitment and survival in rivers: Influence of hydrological processes. Hydrological Process 14(16-17): 3015-3074.

Jönsson, P. & Eklundh, L. (2002). Seasonality extraction and noise removal by function fitting to time-series of satellite sensor data, IEEE Transactions of Geoscience and Remote Sensing, 40(8), 1824-1832.

Jönsson, P., & Eklundh, L. (2004). TIMESAT - a program for analyzing time-series of satellite sensor data. Computers & Geosciences, 30(8), 833-845.

Karnieli, A., Kaufman, Y. J., Remer, L., & Wald, A. (2001). AFRI - Aerosol free vegetation index. Remote Sensing of Environment, 77(1), 10-21.

Kaufman, Y. J., Tanré, D., Remer, L. A., Vermote, E. F., Chu, A., & Holben, B. N. (1997). Operational remote sensing of tropospheric aerosol over land from EOS moderate resolution imaging spectroradiometer. Journal of Geophysical Research: Atmospheres, 102(D14), 17051–17067.

Laben, C. A., & Brower, B. V. (2000). U.S. Patent No. 6,011,875. Washington, DC: U.S. Patent and Trademark Office.

Li, Z., He, L., Zhang, H., Urrutia-Cordero, P., Ekvall, M.K., Hollander, J. & Hansson, L.A., 2017. Climate warming and heat waves affect reproductive strategies and interactions between submerged macrophytes. Global Change Biology, 23(1), pp.108-116.

Loheide, S.P. & Booth, E.G. 2011. Effects of changing channel morphology on vegetation, groundwater, and soil moisture regimes in groundwater-dependent ecosystems. Geomorphology 126(3-4), 364-376.

Luo, J., Li, X., Ma, R., Li, F., Duan, H., Hu, W., Qin, B. and Huang, W., 2016. Applying remote sensing techniques to monitoring seasonal and interannual changes of aquatic vegetation in Taihu Lake, China. Ecological Indicators, 60, 503-513.

Lymburner, L., Beggs, P. J., & Jacobson, C. R. (2000). Estimation of canopy-average surface-specific leaf area using Landsat TM data. Photogrammetric Engineering and Remote Sensing, 66(2), 183-192.

Malthus, T. J. (2017). Bio-optical modeling and remote sensing of aquatic macrophytes. Bio-optical Modeling and Remote Sensing of Inland Waters, pp. 263.

Maxwell, S. K., Schmidt, G. L., & Storey, J. C. (2007). A multi-scale segmentation approach to filling gaps in Landsat ETM+ SLC-off images. International Journal of Remote Sensing, 28(23), 5339-5356.

Merritt, D.M., Scott, M.L., LeRoy, Poff N., Auble, G.T., & Lytle, D.A. 2010. Theory, methods and tools for determining environmental flows for riparian vegetation: Riparian vegetation-flow response guilds. Freshwater Biology 55(1): 206-225.

Netten, J. J., Van Zuidam, J., Kosten, S., & Peeters, E. T. (2011). Differential response to climatic variation of free-floating and submerged macrophytes in ditches. Freshwater Biology, 56(9), 1761-1768.

Received 3 October 2017, Accepted 27 June 2018, Available online 11 July 2018 (**embargo expires 11 July 2020**)

Published version available at: https://doi.org/10.1016/j.rse.2018.06.048

Paillisson J.M., & Marion L. (2006). Can small water level fluctuations affect the biomass of Nymphaea alba in large lakes? Aquatic Botany, 84, 259-266.

Peel, M.C., Finlayson, B.L., & McMahon, T.A. (2007). Updated world map of the Köppen-Geiger climate classification. Hydrology and Earth System Sciences, 11, 1633–1644.

Peeters, E. T., Zuidam, J. P., Zuidam, B. G., Nes, E. H., Kosten, S., Heuts, P. G., Roijackers, R. M. M., Netten, J. C. & Scheffer, M. (2013). Changing weather conditions and floating plants in temperate drainage ditches. Journal of Applied Ecology, 50(3), 585-593.

Pinardi M, Bartoli M, Longhi D, Viaroli P, 2011. Net autotrophy in a fluvial lake: The relative role of phytoplankton and floating-leaved macrophytes. Aquatic Sciences, 73(3):389-403.

Pinardi, M., Fenocchi, A., Giardino, C., Sibilla, S., Bartoli, M., & Bresciani, M. (2015). Assessing potential algal blooms in a shallow fluvial lake by combining hydrodynamic modelling and remote-sensed images. Water, 7(5), 1921-1942.

Reed, B. C., Brown, J. F., VanderZee, D., Loveland, T. R., Merchant, J. W., & Ohlen, D. O. (1994). Measuring phenological variability from satellite imagery. Journal of Vegetation Science, 5(5), 703-714.

Reed, B.C., 2006. Trend analysis of time-series phenology of North America derived from satellite data. GIScience & Remote Sensing, 43(1), pp.24-38.

Richardson, A. D., Keenan, T. F., Migliavacca, M., Ryu, Y., Sonnentag, O., & Toomey, M. (2013). Climate change, phenology, and phenological control of vegetation feedbacks to the climate system. Agricultural and Forest Meteorology, 169, 156-173.

Richter R., & D. Schläpfer (2011). Atmospheric/Topographic Correction for Satellite Imagery, DLR report DLR-IB 565-02/11, Wessling (D), pp 202.

Rouse Jr, J., Haas, R. H., Schell, J. A., & Deering, D. W. (1974). Monitoring vegetation systems in the Great Plains with ERTS. NASA Special Publication, 351, 309.

Sletvold, N., Ågren, J. (2015). Climate-dependent costs of reproduction: Survival and fecundity costs decline with length of the growing season and summer temperature. Ecology Letters, 18, 357-364.

SWB 2015. Database and information materials of the "Parcul Natural Balta Mica a Brailei". http://bio.geoportal-mediu.ro/viewer/bmb/, accessed in September 2015.

Tan, B., Morisette, J. T., Wolfe, R. E., Gao, F., Ederer, G. A., Nightingale, J., & Pedelty, J. A. (2011). An enhanced TIMESAT algorithm for estimating vegetation phenology metrics from MODIS data. IEEE Journal of Selected Topics in Applied Earth Observations and Remote Sensing, 4(2), 361-371.

Tian Y.C., Zhu Y., Cao W.X. (2005). Monitoring soluble sugar, total nitrogen & its ratio in wheat leaves with canopy spectral reflectance. Acta Agronomica sinica, 31: 355-360.

Villa, P., Boschetti, M., Morse, J. L., & Politte, N. (2012). A multitemporal analysis of tsunami impact on coastal vegetation using remote sensing: A case study on Koh Phra Thong Island, Thailand. Natural Hazards, 64(1), 667-689.

Villa, P., Bresciani, M., Bolpagni, R., Pinardi, M., & Giardino, C. (2015). A rule-based approach for mapping macrophyte communities using multi-temporal aquatic vegetation indices. Remote Sensing of Environment, 171, 218-233.

Villa, P., Mousivand, A., & Bresciani, M. (2014). Aquatic vegetation indices assessment through radiative transfer modeling and linear mixture simulation. International Journal of Applied Earth Observation and Geoinformation, 30, 113-127.

Villa, P., Pinardi, M., Tóth, V. R., Hunter, P. D., Bolpagni, R., & Bresciani, M. (2017). Remote sensing of macrophyte morphological traits: Implications for the management of shallow lakes. Journal of Limnology, 76(s1), 109-126.

Wang L., Dronova I., Gong P., Yang W., Li Y. Liu, Q. 2012. A new time series vegetation-water index of phenological-hydrological trait across species and functional types for Poyang Lake wetland ecosystem. Remote Sensing of Environment, 125, 49-63.

Weiss, M., Baret, F., Smith, G. J., Jonckheere, I., & Coppin, P. (2004). Review of methods for in situ leaf area index (LAI) determination: Part II. Estimation of LAI, errors and sampling. Agricultural and Forest Meteorology, 121(1-2), 37-53.

White, M. A., & Nemani, A. R. (2003). Canopy duration has little influence on annual carbon storage in the deciduous broad leaf forest. Global Change Biology, 9(7), 967−972.

Wolkovich, E. M., & Cleland, E. E. (2011). The phenology of plant invasions: A community ecology perspective. Frontiers in Ecology and the Environment, 9(5), 287-294.

Yang, Y., Guan, H., Shen, M., Liang, W. and Jiang, L., 2015. Changes in autumn vegetation dormancy onset date and the climate controls across temperate ecosystems in China from 1982 to 2010. Global Change Biology, 21(2),

Received 3 October 2017, Accepted 27 June 2018, Available online 11 July 2018 (**embargo expires 11 July 2020**)

Published version available at: https://doi.org/10.1016/j.rse.2018.06.048

652-665.

Zhang X., Odgaard R., Olesen B., Lauridsen T.L., Liboriussen L.,Søndergaard M., Liu Z., Jeppesen E. (2015). Warming shows differential effects on late-season growth and competitive capacity of Elodea canadensis and Potamogeton crispus in shallow lakes. Inland Waters, 5(4): 421-432.

Zhang, X., Friedl, M. A., Schaaf, C. B., Strahler, A. H., Hodges, J. C., Gao, F., Reed, B. C. & Huete, A. (2003). Monitoring vegetation phenology using MODIS. Remote Sensing of Environment, 84(3), 471-475.

Zinke P, Aberle J, Nedelcut F (2016) Vegetation changes at "Fundu Mare Island" in the Inner Danube Delta near Brăila (Romania). River Flow 2016, 2174–2181.

Received 3 October 2017, Accepted 27 June 2018, Available online 11 July 2018 (**embargo expires 11 July 2020**)